

DEPARTMENT OF INFORMATION TECHNOLOGY AND  
ELECTRICAL ENGINEERING

Spring Semester 2022

# Single anchor localisation using BLE Angle of Arrival & UWB Ranging

Semester Thesis

Nando Galliard Bsc  
gnando@student.ethz.ch

April 2022

Supervisors: Silvano Cortesi Msc, [silvano.cortesi@pbl.ee.ethz.ch](mailto:silvano.cortesi@pbl.ee.ethz.ch)  
Dr. Michele Magno, [michele.magno@pbl.ee.ethz.ch](mailto:michele.magno@pbl.ee.ethz.ch)  
Professor: Prof. Dr. Luca Benini, [lbenini@ethz.ch](mailto:lbenini@ethz.ch)

# Acknowledgements

I would like to begin this report by thanking several people who helped me greatly during this semester project. Firstly I would like to thank my two supervisors Dr. Michele Magno and Silvano Cortesi, for their support and guidance during this project. I would also like to thank Dr. Christian Vogt, Elio Reinschmidt, Federico Villani and Lukas Schulthess for their knowledge and support in embedded IoT design and the Zephyr RTOS.

# Abstract

Finding your bearings in an unfamiliar space has become easier than ever with global navigation satellite system (GNSS)s. Yet, these systems are not available for an indoor use case. For a hospital to keep track of their x-ray machines or a factory to know the location of all their toolkits there needs to be a more precise solution. While good accuracy is always desirable, it is also imperative for internet of things (IoT) edge devices to keep low energy consumption.

This work develops an indoor localisation system by fusing two localisation techniques. Firstly a Bluetooth based localisation system designed by the company u-blox, and secondly, an ultra-wide band (UWB) system designed by Qorvo. Combining these two systems has the benefit that only one anchor is necessary for complete localisation in polar coordinates in contrast to three or more anchors for any of these systems alone. The novel indoor localisation system is then evaluated using a state-of-the-art optical motion capture system by Vicon.

It is shown that our implementation of the distance ranging component of the system performs very well and that the Bluetooth angle detection has problems intrinsic to the u-blox implementation with disruptive factors such as multipath propagation.

# Declaration of Originality

I hereby confirm that I am the sole author of the written work here enclosed and that I have compiled it in my own words. Parts excepted are corrections of form and content by the supervisor. For a detailed version of the declaration of originality, please refer to Appendix B

Nando Galliard Bsc,  
Zurich, April 2022



# Contents

<b>List of Acronyms</b>	<b>xi</b>
<b>1. Introduction</b>	<b>1</b>
<b>2. Related Work</b>	<b>3</b>
2.1. Indoor tracking technologies . . . . .	3
2.2. Single Anchor Localisation Implementations . . . . .	4
<b>3. Fundamentals</b>	<b>6</b>
3.1. Bluetooth Low Energy Localisation . . . . .	6
3.1.1. Signals Strength Indication . . . . .	6
3.1.2. Angle Of Arrival . . . . .	7
3.1.3. Angle Of Departure . . . . .	8
3.1.4. Bluetooth Direction Finding Signals . . . . .	9
3.1.5. Eddystone . . . . .	10
3.1.6. Bluetooth Advertisements . . . . .	10
3.2. Ultra-wide Band Ranging . . . . .	11
3.2.1. Distance Measurement Techniques With UWB . . . . .	11
3.2.2. Double-sided Two-way Ranging . . . . .	12
3.2.3. Single-sided two-way ranging . . . . .	12
3.3. Zephyr RTOS Operating system . . . . .	13
3.3.1. External Module Instruction . . . . .	13
3.3.2. Folder Structure . . . . .	14
<b>4. Implementation Of Localisation</b>	
<b>Beacon &amp; Anchor</b>	<b>16</b>
4.1. Anchor Design . . . . .	16
4.2. Custom Beacon Board . . . . .	17
4.2.1. MCU And Bluetooth Radio . . . . .	18
4.2.2. UWB Radio Module . . . . .	18

## Contents

4.2.3. Utilities . . . . .	18
4.3. Block Diagram Of Components . . . . .	19
<b>5. Firmware Of Beacon And Anchor</b>	<b>20</b>
5.1. Threads . . . . .	20
5.1.1. Bluetooth Advertisements . . . . .	20
5.2. UWB Ranging Exchange . . . . .	21
5.3. Logging Software . . . . .	21
5.4. Fusion Of AoA And Distance Data Algorithm . . . . .	23
5.4.1. Coordinate Transformations . . . . .	23
<b>6. Experimental Setup</b>	<b>25</b>
6.1. Definition Of Ground Truth - Vicon . . . . .	25
6.1.1. Room Setup For Measurements . . . . .	25
6.1.2. Setup Of Vicon System . . . . .	26
6.1.3. Setup Of Anchor . . . . .	27
6.1.4. Setup of Beacon . . . . .	27
6.2. Central Static Measurements . . . . .	28
6.3. Dynamic Measurement . . . . .	28
<b>7. Results</b>	<b>29</b>
7.0.1. Results For Central Static Measurements . . . . .	29
7.0.2. Experiment Location #2 Low . . . . .	29
7.0.3. Experiment Location #2 Low, Setup Moved -X Direction . . . . .	31
7.0.4. Experiment Location #9 High . . . . .	33
7.0.5. Experiment Location #6 Low . . . . .	34
7.0.6. Experiment Location #7 Low . . . . .	35
7.0.7. Experiment Location #3 High . . . . .	36
7.0.8. Results Dynamic Measurement Circular . . . . .	37
7.0.9. Results Dynamic Measurement Height . . . . .	38
<b>8. Discussion</b>	<b>39</b>
<b>9. Conclusion</b>	<b>42</b>
9.1. Future Work . . . . .	43
<b>A. Task Description</b>	<b>44</b>
<b>B. Declaration of Originality</b>	<b>48</b>
<b>C. File Structure</b>	<b>49</b>
<b>D. Beacon Schematic</b>	<b>51</b>

*Contents*

<b>E. Zephyr Code Appendix</b>	<b>55</b>
E.1. Application . . . . .	55
E.2. Modules . . . . .	55
<b>F. Remaining Plots</b>	<b>57</b>
<b>Glossary</b>	<b>65</b>

# List of Figures

3.1.	AoA illustration. Two antennas in array at receiver. Blue lines represent radio signals with wavelength $\lambda$ .	8
3.2.	AoD illustration. Two antennas in array at the transmitter. Blue lines represent radio signals with wavelength $\lambda$ .	9
3.3.	Bluetooth direction finding signal packet with constant tone extension.	10
3.4.	The makeup of the four Eddystone beacon packages.	10
3.5.	Two-way ranging exchange.	13
4.1.	C211 board from u-blox [1]	17
4.2.	Elevation and azimuth angles in relation to C211.	17
4.3.	The custom made beacon board by Silvano Cortesi MSc.	17
4.4.	Simplified block diagram of the beacon PCB.	19
5.1.	Ultra-wideband packages sent by ranging exchange.	22
5.2.	Azimuth, elevation angles and distance vector in relation to center of anchor.	23
6.1.	Floorplan of the test room with world coordinate origin at the middle of the room on floor level below where the anchor is located.	26
6.2.	Anchor mount for the experiment.	28
6.3.	The custom beacon board is encased in the C209 case and prepared for the Vicon system.	28
7.1.	Histogram Experiment Location 2L	30
7.2.	Cartesian Representation Experiment Location 2L	30
7.3.	Cartesian Representation Experiment Location 2L Changed	31
7.4.	Histogram Experiment Location 2L Changed	31
7.5.	Distance, Azimuth and Elevation Delta Over Experiment Location 2L Changed	32
7.6.	Cartesian Representation Experiment Location 9H	33
7.7.	Histogram Experiment Location 9H	33

*List of Figures*

7.8. Cartesian Representation Experiment Location 6L . . . . .	34
7.9. Histogram Experiment Location 6L . . . . .	34
7.10. Cartesian Representation Experiment Location 7L . . . . .	35
7.11. Histogram Experiment Location 7L . . . . .	35
7.12. Cartesian Representation Experiment Location 3H . . . . .	36
7.13. Histogram Experiment Location 3H . . . . .	36
7.14. Dynamic circle measurement in Cartesian coordinates. . . . .	37
7.15. Dynamic height measurement in Cartesian coordinates. . . . .	38
8.1. Illustration of multipath propagation. . . . .	40
8.2. Illustration of impact of reflected waves on the measured signal. . . . .	41
F.9. 01 Mai Experiment Position 7 Histogram Plot . . . . .	57
F.10.01 Mai Experiment Position 7 Position Plot . . . . .	58
F.1. 01 Mai Experiment Position 1 Position Plot . . . . .	59
F.2. 01 Mai Experiment Position 2 Position Plot . . . . .	59
F.3. 01 Mai Experiment Position 5 Position Plot . . . . .	59
F.4. 01 Mai Experiment Position 6 Position Plot . . . . .	59
F.5. 01 Mai Experiment Position 1 Histogram Plot . . . . .	60
F.6. 01 Mai Experiment Position 2 Histogram Plot . . . . .	60
F.7. 01 Mai Experiment Position 5 Histogram Plot . . . . .	60
F.8. 01 Mai Experiment Position 6 Histogram Plot . . . . .	60
F.11.08 Mai Experiment Position 2 Position Plot . . . . .	61
F.12.08 Mai Experiment Position 3 Position Plot . . . . .	61
F.13.08 Mai Experiment Position 4 Position Plot . . . . .	61
F.14.08 Mai Experiment Position 5 Position Plot . . . . .	61
F.15.08 Mai Experiment Position 2 Histogram Plot . . . . .	62
F.16.08 Mai Experiment Position 3 Histogram Plot . . . . .	62
F.17.08 Mai Experiment Position 4 Histogram Plot . . . . .	62
F.18.08 Mai Experiment Position 5 Histogram Plot . . . . .	62
F.19.08 Mai Experiment Position 8 Position Plot . . . . .	63
F.20.08 Mai Experiment Position 9 Position Plot . . . . .	63
F.21.08 Mai Experiment Position 8 Histogram Plot . . . . .	63
F.22.08 Mai Experiment Position 9 Histogram Plot . . . . .	63
F.23.08 Mai Dynamic Experiment 1 Plot . . . . .	64
F.24.08 Mai Dynamic Experiment 2 Plot . . . . .	64
F.25.08 Mai Dynamic Experiment 3 Plot . . . . .	64
F.26.08 Mai Dynamic Experiment 4 Plot . . . . .	64

# List of Tables

2.1. Results from different related work. . . . .	5
3.1. UWB frequency band standards utilised in different regions. [2] . . . . .	11
6.1. Test room dimensions measured outwards from floor level under anchor location. . . . .	27

# List of Acronyms

AA . . . . .	access address
AoA . . . . .	angle of arrival
AoD . . . . .	angle of departure
BLE . . . . .	Bluetooth low energy
CRC . . . . .	cyclic redundancy check
CTE . . . . .	constant tone extension
GF . . . . .	gaussian filter
GNSS . . . . .	global navigation satellite system
IC . . . . .	Integrated Circuit
IMU . . . . .	inertial measurement unit
IoT . . . . .	internet of things
IQ . . . . .	in-phase and quadrature
ISM . . . . .	industrial, scientific and medical band
MUSIC . . . . .	multiple signal classification
NRLS . . . . .	nonlinear recursive least squares
PCB . . . . .	printed circuit board

*List of Acronyms*

PDU . . . . .	protocol data unit / payload of
RF . . . . .	radio frequency
RSSI . . . . .	received signal strength indicator
RTOS . . . . .	real time operating system
SAL . . . . .	single anchor localisation
SI . . . . .	simple identification
SIG . . . . .	Bluetooth special interest group
UKF . . . . .	unscented Kalman filter
UWB . . . . .	ultra-wide band
WPAN . . . . .	wireless personal area network
Zephyr . . . . .	Zephyr real time operating system



# Chapter 1

## Introduction

Finding your bearing in an unfamiliar space has become easier than ever with global navigation satellite system (GNSS)s, yet these systems are unavailable indoors. If a student wants to find the correct classroom on a new campus, a hospital, a missing x-ray machine or a factory, a tool GNSS will not suffice since the satellite radio frequency (RF) signal is not strong enough to penetrate the walls or ground. Indoor localisation is needed to achieve this. Systems to localise oneself in an indoor environment already exist! Technologies like Bluetooth and ultra-wide band (UWB) are already implemented in most smartphones and can serve as a beacon for localisation if implemented in positioning apps. These technologies utilise triangulation and trilateration, which in essence, means that one needs to have a line of sight to at least three different anchor nodes to begin localisation. Having multiple anchors per room drives up the cost and complexity of equipping a building to engage in indoor localisation while also creating an unnecessary amount of message exchanges.

In this work, we aim to develop a single anchor solution equipped with the means to singlehandedly localise a beacon in its line of sight that can send Bluetooth low energy (BLE) and UWB RF signals. While good accuracy is desirable, we also want to strive for low energy consumption to enable usage of this system on edge devices of the internet of things (IoT). As noted before, multiple systems on the market are able to do either angle detection or distance ranging. Thus we seek to build a sensor fusion anchor out of these systems.

## *1. Introduction*

Thus this thesis aims to acquire angle of arrival (AoA) using BLE direction finding and distance information using ultra-wide band. This aim includes the creation of a board file for the Zephyr real time operating system for a PCB designed in previous work and the porting of a driver for the UWB sensor into Zephyr. In a second step, combine these two pieces of information and perform a localisation. In the last step, we evaluate the performance of this sensor fusion system.

The detailed task description can be found in appendix A.

# Chapter 2

## Related Work

### 2.1. Indoor tracking technologies

There have been many radio frequency (RF) technologies investigated for indoor localisation, like Wi-Fi [3], IEEE 802.15.4 [4][5], Bluetooth [6][7] and ultra-wide band (UWB) [8]. Yet these systems, without further handling, achieve only precision in the meter range while still needing a high amount of anchors and thus also needing a lot of work to deploy.

Efficient positioning can be achieved by estimating the angle of arrival (AoA) of multi-antenna arrays, as discussed by He et al [9], by using signal processing. The researcher argued that the AoA approach is sensitive to noise, multipath, and path loss phenomena. Pertaining to this, they designed a signal processing method with nonlinear recursive least squares (NRLS) and an unscented Kalman filter (UKF) to solve these issues of AoA. This signal processing stands adverse to the classical multiple signal classification (MUSIC) and improves the average estimation error of the AoA calculated by 3.9 degrees, an improvement of 44 % in contrast to MUSIC. The same approach was taken by Hajiakhondi et al. [10] with the addition of a gaussian filter (GF). They noted general errors of at most 10 degrees but took notice of a considerable error from  $\pm$  (60 to 90) degrees, meaning near parallel to their antenna setup.

Monfared et al. [11] developed a multi anchor iterative localisation method that employs AoA for a first estimation of position and then improves this by using received signal strength indicator (RSSI) to estimate the distance. Detailed mathematical derivations of the iterative algorithm are presented. The researchers achieved an accuracy of 1.8 meters at 80% accuracy.

## 2.2. Single Anchor Localisation Implementations

A paper that recognised the simplicity of using a single anchor was Wang et al. [12]. The researchers theorised that using distance and angle measurements, one could locate an object in 3D space, in essence using polar coordinates. They additionally extended this theory for multiple anchors by developing an algorithm that means the data points to improve the accuracy of the final location by only incurring a linear runtime growth. They evaluated this theory by simulating measured data points with random error deltas. Finally, they concluded that their algorithm has superior performance to classical triangulation or trilateration systems. The researchers did no real-world experiment, and no prototype was implemented.

The researchers Großwindhager et al. [13] utilised a single anchor node with four UWB antennas to achieve AoA and two-way distance ranging. Their most significant contribution to the field is a novel SALMA model that utilised the usually destructive properties of multipath propagation to its advantage. The SALMA model only requires a crude floor print of the room it will be stationed in to calculate possible multipath propagation to factor into its calculations. With this technique, they achieve a median error of 9.85 cm and a 90% error of 50 cm.

Wang et al. [14] also developed a SAL method with UWB AoA and two-way distance ranging but focused on a theoretically unlimited amount of beacons. A conventional ranging protocol requires at least  $2N + 1$  UWB signals for an  $N$ -beacon system. Their implementation uses a minimum of  $N + 2$  signals and the concept of (quasi-)simultaneous response, enabling the anchor to receive all the agent responses in one estimated channel impulse response and enabling this SAL method.

## 2. Related Work

Author	Tech	# Anchors	# Beacons	Real or Sim	Median –	90% precision
He et al [9]	BLE	3 +	1	Real	5 deg	–
Hajikhondi et al. [10]	BLE	3 +	1	Real	8 deg	–
Monfared et al. [11]	–	3 +	1	Sim	–	1.8 m
Wang et al. [12]	–	1 +	1	Sim	–	–
Großwindhager et al. [13]	UWB	1	1	Real	9.85 cm	50 cm
Wang et al. [14]	UWB	1	$\infty$	Real	6.5 cm	13.6 cm

Table 2.1.: Results from different related work.

# Chapter 3

## Fundamentals

This chapter represents a refresher for the uncertain reader about any protocols or techniques used to develop the single anchor localisation system.

### 3.1. Bluetooth Low Energy Localisation

Bluetooth is a widely available and broadly used short-range communication protocol. Bluetooth low energy (BLE) is a variant of this protocol introduced by the Bluetooth special interest group (SIG) with Bluetooth v4.0 intended for edge devices with steeper energy consumption requirements. BLE uses the industrial, scientific and medical band (ISM) at 2.4 GHz, divided into 40 2 MHz channels. In contrast, Bluetooth Classic uses 79 1 MHz channels at the same frequency band [15][16]. During a connection, the devices use 37 available channels with adaptive frequency hopping, while the remaining three channels are dedicated to advertising. With Bluetooth v5.0 and extended advertising, all 40 radio channels are used as data channels. For one localisation connection with BLE, there are two roles. One stationary anchor where the location is known and one beacon that has yet to be located.

#### 3.1.1. Signals Strength Indication

The first way to estimate ones location with BLE was the reception strength of a received signal. While it is too imprecise for this work, we include this short chapter for completeness. RSSI based localisation estimates the distance of the beacon from the anchor by calculating the path loss on the received signal strength, hence the name. This signal strength loss over distance relies heavily on the chipset vendors and differences in radio circuits. Additionally, RSSI is reliant on a path-loss model suited to each location.

### 3. Fundamentals

Thus, in general, RSSI offers only a rough distance estimation with accuracy in the range of multiple meters [17]. With the deployment of multiple known anchors over the desired area, one can localise a Bluetooth device utilising trilateration. This trilateration approach is not suited for this work and will thus not be further discussed.

#### 3.1.2. Angle Of Arrival

With the release of Bluetooth Core Specification v5.1, support was added for high-accuracy direction-finding. By receiving a single radio signal multiple times via a connected multi-antenna array, one can calculate the angle from which the signal originated, the so-called angle of arrival (AoA). With AoA, the transmitter sends a unique prolonged direction finding signal, explained in the chapter 3.1.4, which gets in-phase and quadrature (IQ) sampled by a receiver equipped with multiple antennas, as seen in figure 3.1. The reception angle  $\theta$  can be calculated with the predefined frequency channel of the radio signal and thus the wavelength  $\lambda$  and the known distance  $d$  between the antennas. Then the only thing needing to be measured is the phase difference  $\psi$  between of the signal between the antennas. This calculation is shown for two dimensions in equation 3.1 [18].

$$\text{Angle of arrival } \theta = \arccos\left(\frac{\psi \cdot \lambda}{2 \cdot \pi \cdot d}\right) \quad (3.1)$$

One must consider that the maximum span of all antennas in an array must be compressed into one wavelength. Additionally, the two actors need to be far enough apart from each other that the system can be described as far-field. It would be possible also to calculate a near field localisation system, but it adds a sizeable geometric complexity to the system. The complete collection process and subsequent calculation of the angle in 3D space are not part of this work since prefabricated units that feature built-in computation units were employed.

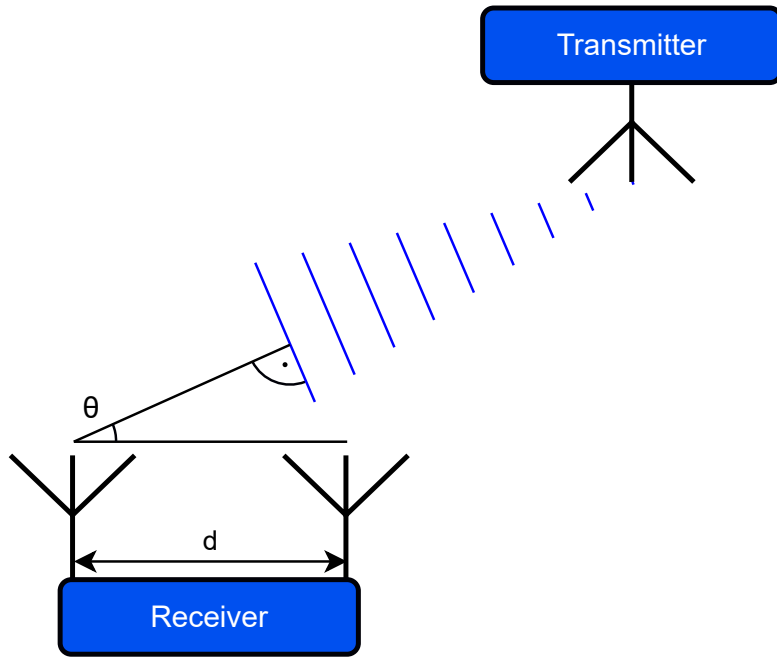


Figure 3.1.: AoA illustration. Two antennas in array at receiver. Blue lines represent radio signals with wavelength  $\lambda$ .

### 3.1.3. Angle Of Departure

There is also a technique where the transmitter employs the antenna array, which we present here for completeness. With angle of departure (AoD), the roles are reversed, and the static anchor utilises a single antenna while the mobile beacon is equipped with an antenna array, as seen in figure 3.2. By IQ sampling the incoming radio signals from all the antennas and knowing the distance  $d$  between the antennas of the array, the anchor can discern the phase changes  $\phi$  between the signals from which it calculates the angle of departure  $\Theta$  as shown for two dimensions in equation 3.2 [18].

$$\text{Angle of departure } \theta = \arcsin \left( \frac{\psi \cdot \lambda}{2 \cdot \pi \cdot d} \right) \quad (3.2)$$

This technique is desirable when the location of one single beacon needs to be as reliable as possible since the anchors can be cheaply deployed in large quantities. In contrast, the more expensive beacon uses the antenna array.



### 3. Fundamentals

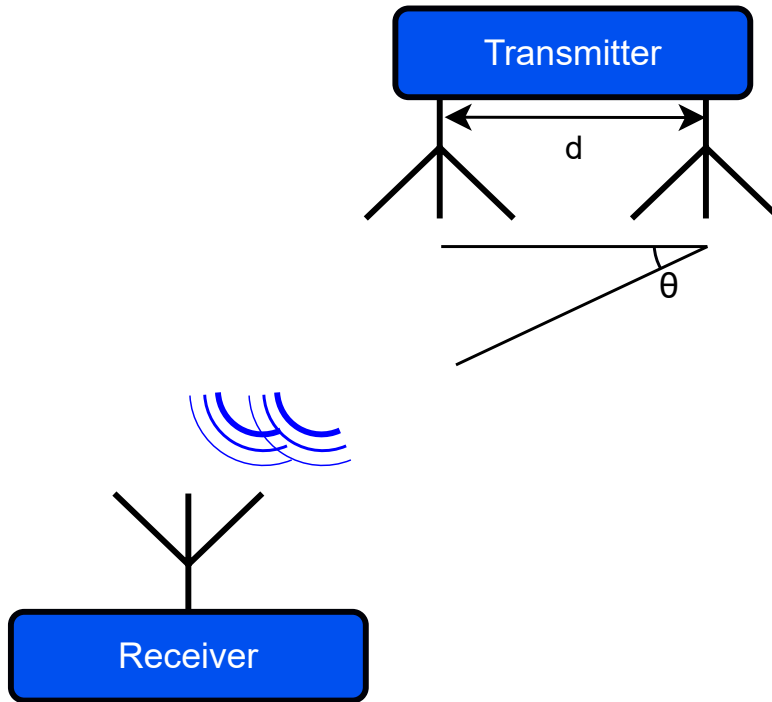


Figure 3.2.: AoD illustration. Two antennas in array at the transmitter. Blue lines represent radio signals with wavelength  $\lambda$ .

#### 3.1.4. Bluetooth Direction Finding Signals

The packages in Bluetooth have the same structure for advertisements and data transmission [19] for ease of use. The packet consists of four components, as shown in figure 3.3. First the preamble is an alternating set of ones and zeroes used for frequency synchronisation, automatic gain control training, and symbol timing estimation to tune the receiver. Secondly, the access address (AA) is sent. Each connection between two devices has a distinct address to distinguish the transmission. Thirdly the protocol data unit / payload of (PDU) gets sent, which includes the length of the payload and the payload itself. Lastly, a cyclic redundancy check (CRC) is calculated from the PDU to guarantee the correct transmission of the payload. If the payload is encrypted, the CRC gets calculated after encryption.

Direction finding signals in BLE are link-layer packets with a constant signal added at the end, a so-called constant tone extension (CTE). Bluetooth sends data via frequency modulation by adding or removing a value defined as frequency deviation  $\Delta f$ . When the channel frequency is defined as  $F_{CH}$  an information bit equal to one is sent at frequency  $F_{CH} + \Delta f$  and respectively a zero is sent at  $F_{CH} - \Delta f$ . Consequently, changing the frequency also changes the wavelength, which is essential for calculating the angle of arrival, as seen in chapter 3.1.2. Thus the CTE is defined as a long sequence (16 to 160

### 3. Fundamentals

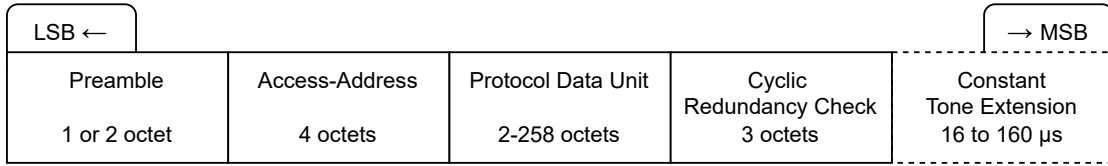


Figure 3.3.: Bluetooth direction finding signal packet with constant tone extension.

$\mu$ s) of digital ones to guarantee the transmission is sent at one frequency and hence the wavelength does not change over the sampling period.

#### 3.1.5. Eddystone

Eddystone is a Bluetooth low energy beacon protocol designed by Google to specifically be used for proximity beacon messaging that can be sent in the payload of a Bluetooth message [20]. In total, there are four different frame types for different use cases. Broadcasting simple (UID) or encrypted identification (EID), URL or website addresses (URL) or telemetry information (TLM).

To satisfy the filtering algorithm of the u-blox anchor, it is sufficient to employ only the simple identification frame designated UID. Figure 3.4 shows the complete structure and the advertisement frame that the protocol expects.

#### 3.1.6. Bluetooth Advertisements

Bluetooth v5.1 was introduced in January of 2019 by the Bluetooth SIG, and with it, the constant tone extension used for angle of arrival localisation, as discussed in chapter 3.1. With the existence of an official standard from the Bluetooth special interest group (SIG),

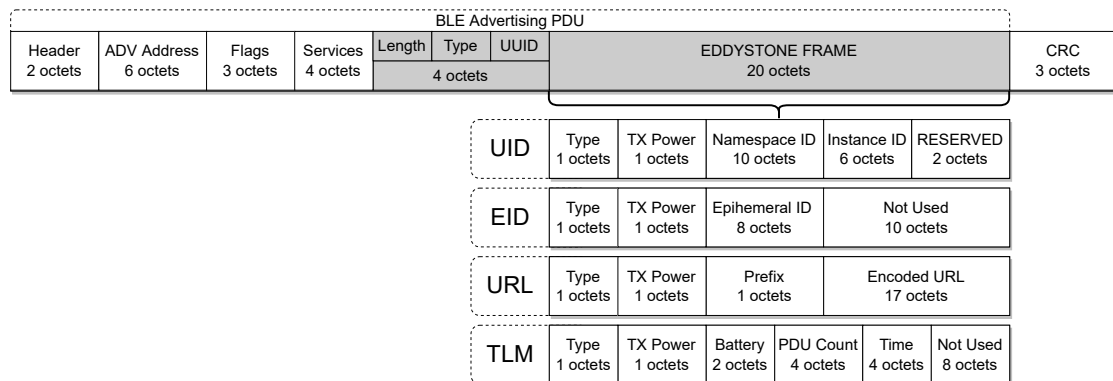


Figure 3.4.: The makeup of the four Eddystone beacon packages.

### 3. Fundamentals

Country	Frequency Bands with restrictions	FB without restrictions
Europe	3.1–4.8 GHz	6–8.5 GHz
North America	-	3.1–10.6 GHz
Japan	3.4–4.8 GHz	7.25–10.2 GHz
Korea	3.4–4.8 GHz	7.2–10.2 GHz
Singapore	6–9 GHz	3.4–4.2 GHz

Table 3.1.: UWB frequency band standards utilised in different regions. [2]

it seems confusing that u-blox made their own implementation of the CTE protocol. One needs to utilise this different implementation to be accepted by the C211 anchor. This is achieved by applying a patch to the radio routine of zephyr as shown in the git of the C209 beacon [21]. For any other version of Zephyr there is also a patch difference file to apply the patch version independent.

## 3.2. Ultra-wide Band Ranging

ultra-wide band (UWB) is another radio technology specialising in low energy consumption, high-bandwidth and short-range transmissions. The UWB standards frequency band is not static and restricted by local laws as shown in Table 3.1 which displays the worldwide differences in frequency bands utilised by UWB. One can see that UWB occupies a wide range in bandwidths thus it must be able to coexist with other narrow-band signals (TV, GPS, GSM, UMTS/3G, etc.). To not create interference for other radio technologies, UWB uses a wide bandwidth range with low emission and an intensity below the power floor of other radio signals. Thus UWB can share the spectrum with existing services [22].

### 3.2.1. Distance Measurement Techniques With UWB

Using RSSI on BLE to perform distance calculations between two devices leads to poor accuracy in the range of multiple meters. This shortcoming is where UWB comes in with time of flight distance calculations. There are two different ways to measure the distance between distinct UWB actors. The following subsections aim is to present an overview of the different techniques used to determine the distance with a ranging exchange where an initiator exchanged multiple messages with a responder, and which of those ultimately will be used in this report.

### 3.2.2. Double-sided Two-way Ranging

In double-sided ranging, one has a designated initiator (Beacon) and likewise a designated responder (Anchor), as visible in figure 3.5. The initiator starts the measurement exchange by broadcasting a poll frame via UWB and recording the transmission timestamp (TX1), and then waits a limited time for a response message. The reception timestamp (RX1) is recorded when a responder receives this poll frame. It sends a reception frame back to the initiator containing only an activity code to go on with the ranging exchange. The initiator receives this message and records its reception timestamp (RX2). The responder could only record the last timestamp from the final transmission (TX2) after sending the signal. Since we do not want to send an additional transmission, the initiator sends a timestamp with the message of when it expects the message to be sent. Thus it sends with the final message the timestamps TX1, TX2 and RX2. The responder is then able to work out the estimated distance between the two devices from these four timestamps by knowing the time of flight over the air and this equation 3.3 [23]. Notice the factor  $F_{UUS} = f_C \cdot N$ , which incorporates the clock cycle  $f_C$  of the antenna chip and the sampling number per clock pulse  $N$  for the internal time register. Lastly,  $c$  represents the speed of light. After the ranging exchange is done, only the responder has knowledge of the estimated distance since he has all the necessary timestamps. This could be remedied by sending the RX1 timestamp with the reception frame, as seen in the single-sided two-way ranging exchange.

$$d\{m\} = \frac{RX1 \cdot RX2 - TX1 \cdot TX2}{RX1 + RX2 + TX1 + TX2} \cdot F_{UUS} \cdot c \quad (3.3)$$

### 3.2.3. Single-sided two-way ranging

The initiator ends with the calculated distance in single-sided ranging and incorporates one message fewer than in double-sided ranging. It begins by sending a polling frame and recording its transmission timestamp (TX1). The responder answers with a response frame containing the responders reception (RX1) and transmission (TX2) timestamp. The timestamp TX2 is similarly guessed as in double-sided ranging. The initiator records the last reception timestamp (RX2) and calculates with equation 3.3 the estimated distance. This technique suffers poorer accuracy due to the clock offset between the two actor nodes, and this clock offset needs to be recorded and taken into account to increase precision.

For the purposes of this prototype, the beacon should announce his presence when expected but can be put to sleep if not needed. For this reason and the accuracy loss of single-sided ranging, we went with the double-sided two-way ranging setup where the initiator is the mobile beacon.

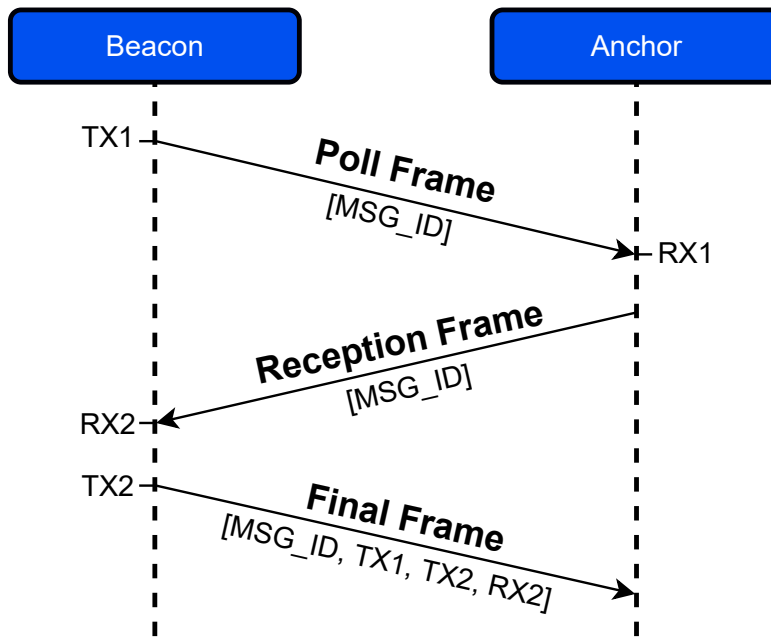


Figure 3.5.: Two-way ranging exchange.

### 3.3. Zephyr RTOS Operating system

The Zephyr OS [24] is a real-time operating system based on a small-footprint kernel source tree built like Unix for use on resource-constrained embedded systems like the internet of things edge devices. It supports multiple architectures and is licensed under Apache 2.0 [25].

#### 3.3.1. External Module Instruction

When one wants to add an own implementation of a zephyr board or driver, one generally adds it into the zephyr root itself. While being the most straightforward implementation, it hinders version control when working in groups or with multiple branches since work in progress drivers or proprietary drivers should not be pushed to zephyr origin.

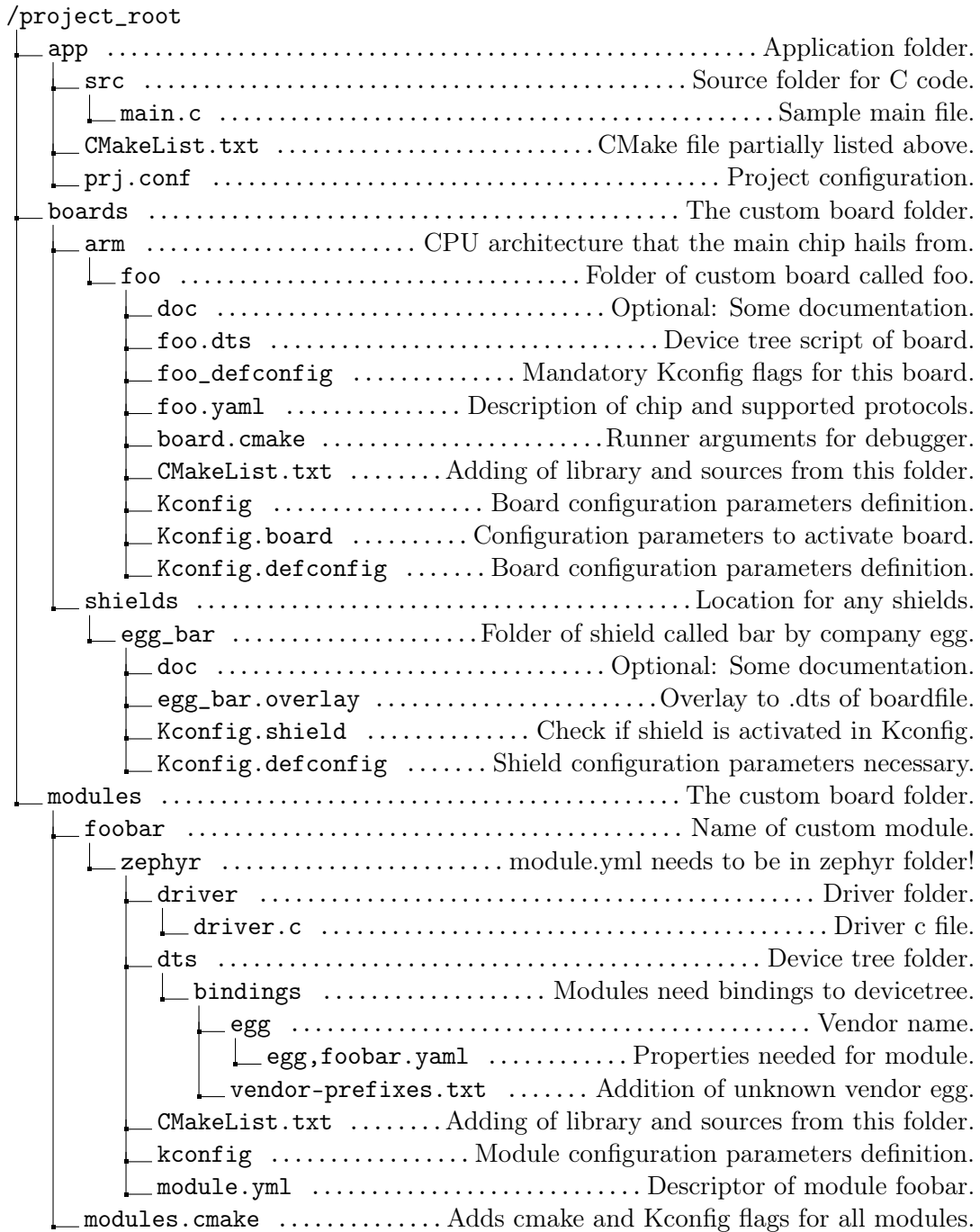
Zephyr has an implementation for this called modules that can be added on compilation from an out of Zephyr tree folder. While the wiki is comprehensive, it still took some work to figure out, and nobody at PBL worked with this technique before thus, we are adding this chapter as a guide for future use. Find the recommended folder structure in subsection 3.3.2 and all relevant files in appendix E.

### 3. Fundamentals

#### 3.3.2. Folder Structure

The best way to start with a custom board is to take the corresponding development board and change its pin connections in the .dts file. A shield can be seen as a modification of the original .dts board file. This application *app* incorporates a custom board *foo*, an additional shield *egg\_bar*, and a module *foobar*. The file content for all relevant files is located in appendix E. We employed two environment variables, `PROJECT_ROOT` gives the path to the project root folder, and `ZEPHYR_BASE` gives the path to the zephyr install location, which the zephyr installation should already create.

### 3. Fundamentals



# Implementation Of Localisation Beacon & Anchor

This section discusses the final implementation of our beacon and single anchor localisation system solution developed in the thesis.

## 4.1. Anchor Design

The Bluetooth anchor consists of the C211 antenna board from the XPLR-AOA-2 evaluation kit designed and distributed by the company u-blox, visible in figure 4.1. It is equipped with an array of five Bluetooth antenna plates arranged in a rectangular fashion compatible with Bluetooth v5.1 and designed for angle of arrival localisation described in section 3.1.2. It also boasts a NINA-B411 Bluetooth module also designed by u-blox that directly calculates the azimuth and elevation angle of a broadcasting beacon relative to the anchor ground plane made up of plate visible in figure 4.2 and outputs these findings over Serial USB. Classically this antenna board is intended to be used with at least three other C211 boards and a C209 beacon board that then gets triangulated. The firmware for the C211 boards is closed source. A user can only marginally configure it by pre-programmed commands to only accept beacon signals with specific Eddystone instance identifications or change the output format, to name a few. In its current implementation the board can reliably distinguish between five different beacons while ignoring further valid signals. [1]. On the other hand, the corresponding beacon boards C209 are open source [21] and a custom implementation can thus be designed.

For the UWB anchor on the other hand no extravagant antenna positioning is needed since we only use a ranging exchange. Thus we can simply mount a small board on the Bluetooth anchor board with preferably the same UWB antenna as the beacon board to



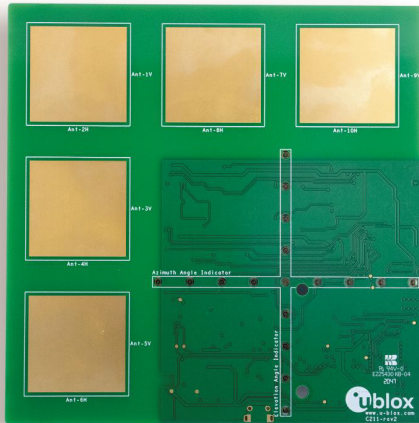


Figure 4.1.: C211 board from u-blox [1]

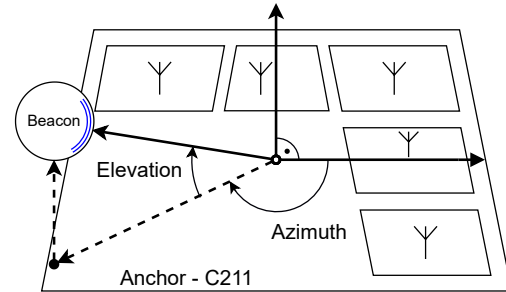


Figure 4.2.: Elevation and azimuth angles in relation to C211.

prevent further uncertainties like differing transmission times etc. For ease of development we used the custom made beacon board described in chapter 4.2 as a UWB anchor and leave the design of a single board with AoA Bluetooth direction finding and UWB ranging exchange for future work.

## 4.2. Custom Beacon Board

The hardware design of the beacon board was done in an earlier project by Silvano Cortesi MSc, one of this thesis's supervisors. The complete schematic for this board is in the appendix D. The goal of this board is to include UWB radio in the same housing used with the original C209 boards while maintaining the liberty of battery-powered freedom, USB enabled recharging and Bluetooth v5.1 radio connections.

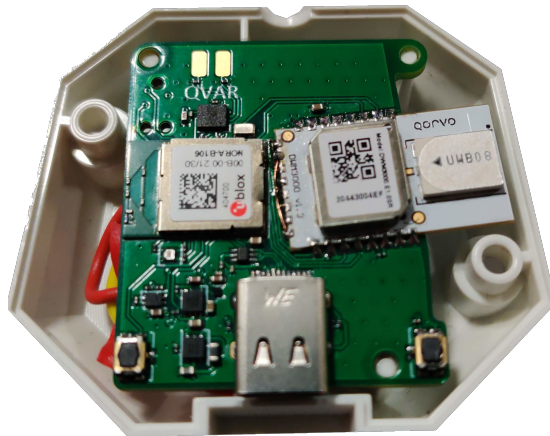


Figure 4.3.: The custom made beacon board by Silvano Cortesi MSc.

### 4.2.1. MCU And Bluetooth Radio

The beacon boards MCU is a u-blox stand-alone dual-core low energy module equipped with Bluetooth v5.2 and IEEE 802.15.4 adequate 2.4 GHz radio [26]. It is based on the Nordic Semiconductor nRF5340 system on chip (SoC) with an ARM Cortex-M33 application and an additional network processor. The nRF5340s application core runs at 128 or 64 MHz and is equipped with 1 MB of flash memory and 512 kB of RAM. The network core, on the other hand, only runs at a maximum of 64 MHz and has 256 kB flash memory and 64 kB RAM. At 3V supply voltage and core benchmark tests running the application core consumes  $62.5 \mu\text{A}/\text{MHz}$  at full 128 MHz clock speed while the network core consumes  $40.6 \mu\text{A}/\text{MHz}$  at full 64 MHz. The whole module is seated in a 48 ball grid array package.

### 4.2.2. UWB Radio Module

To utilise UWB radio on this new board, it is equipped with the Qorvo (formerly Decawave) DWM3000 [27] fully integrated ultra-wideband transceiver module based on the DW3110 integrated circuit (IC). It includes an antenna, RF circuitry, power management, and clock circuitry in the module, making integration more straightforward. It is IEEE 802.15.4-2015 compliant and supports UWB Channel 5 ( $6.5 \text{ GHz} \pm 500\text{MHz}$ ) and Channel 9 ( $8 \text{ GHz} \pm 500\text{MHz}$ ). Lastly, it is controlled via an SPI interface by the host processor.

### 4.2.3. Utilities

Additionally, the board incorporates a battery pack with on board battery monitor and a system in package (SiP) 3D accelerometer and 3D digital gyroscope with the LSM6DSV16X [28] by ST Microelectronics.

### 4.3. Block Diagram Of Components

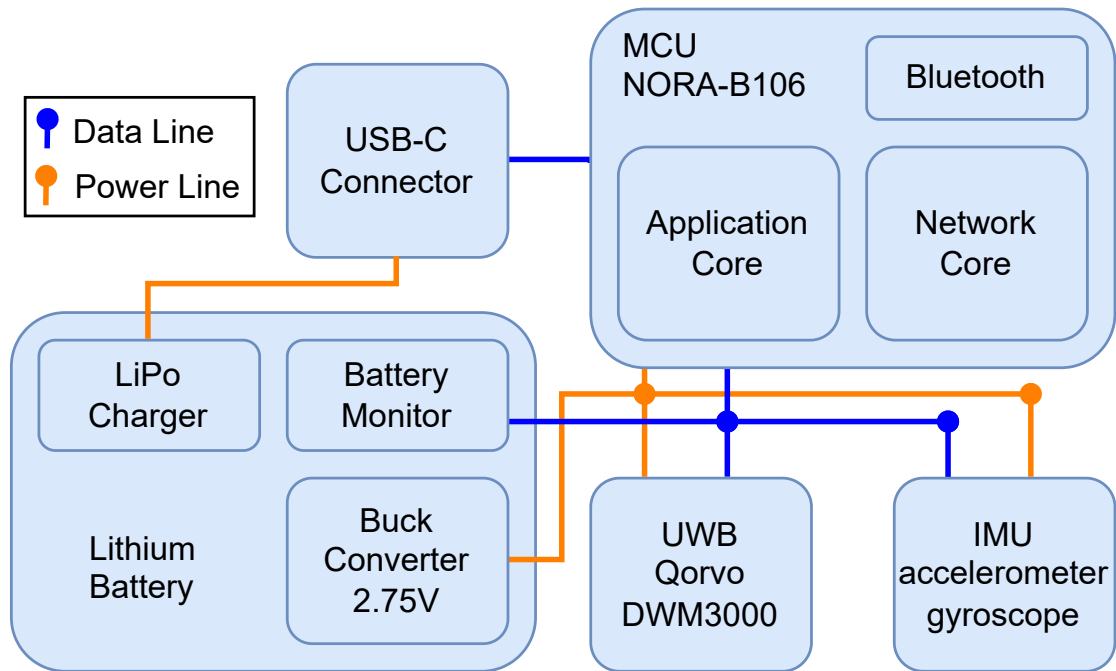


Figure 4.4.: Simplified block diagram of the beacon PCB.

# Chapter 5

## Firmware Of Beacon And Anchor

In this chapter a summary of the firmware implementation is given for the beacon and UWB anchor board is given. The focus is on the protocols used for the transmissions and the algorithms used to calculate the resulting localisation.

### 5.1. Threads

The firmware of the beacon is written with the Zephyr OS. All tasks are assigned to a thread each, one of the advantages of the zephyr RTOS. The advertisement for Bluetooth is initiated on the application core but then all responsibility for the continued transmissions are transferred to the network core.

#### 5.1.1. Bluetooth Advertisements

The antenna array boards designed by u-blox only accept transmissions that get advertised with the unencrypted identification protocol UID defined by the Eddystone protocol discussed in chapter 3.1.5. They also need to contain the correct *namespace* and a variance of the tag id in the *instance id*. Thus the package that we are sending is visible in listing 1.

## 5. Firmware Of Beacon And Anchor

```
bt_data ad[] = {
    BT_DATA_FLAGS, BT_LE_AD_NO_BREDR,    # Flags
    BT_DATA_UUID16_ALL, 0xaa, 0xfe,     # Service
    BT_DATA_SVC_DATA16, 0xaa, 0xfe,     # Eddystone UUID
    0x00,                                # Eddystone-UID frame type
    0x00,                                # TX Power
    'N', 'I', 'N', 'A', '-',           # Namespace fixed
    'B', '4', 'T', 'A', 'G',           # Namespace fixed
    't', 'a', 'g', 'x', 'x', 'x',      # Instance Id, XXX is variable
    0x00, 0x00};                       # reserved per protocol
```

Listing 1: Bluetooth Eddystone frame sent by beacon.

## 5.2. UWB Ranging Exchange

The UWB messages sent by the DWM3000 need to comply with the IEEE 802.15.4 standard MAC data frame encoding to be acceptable for future licensed use.

We use the Double-sided two-way ranging process discussed in the chapter 3.2.2 to determine the distance between the beacon and anchor. For one ranging exchange, we are thus sending three different sequential messages: an initial poll, a response from the responder and the final message. The payload of these three messages is shown in figure 5.1. After a completed exchange, the anchor calculates the expected distance between the two actors using equation 3.3 and sends this information via serial over the onboard USB port. For this build, the destination and source address are hardcoded, and the third octet of the message is set as a sequence number. In an official release, these addresses would need to be dynamically assigned.

## 5.3. Logging Software

The Vicon system is interfaceable by utilising a Python script called ViconWrapper defined in *vicon\_commander.py* provided by Vlad Niculescu (vladn@iis.ee.ethz.ch) on the internal repository [29]. In the file *ex1-main-just-vicon.py*, the traceable objects must be named the same as in the Vicon software. The wrapper is then utilised to log the sampled position of the objects in the hot zone. This CSV logfile records the UTC timestamp, the time since measurement start, and the name of the tracked object with an appendix for the x,y,z position or the quaternions as w,x,y,z and the corresponding value.

At the same time, both the Bluetooth and UWB anchor are outputting data via the serial USB connection. We used the *parser\_ble.py* and *parser\_uwb.py* included in this works git under the Software folder visible in the appendix C to log this data. The CSV

5. Firmware Of Beacon And Anchor

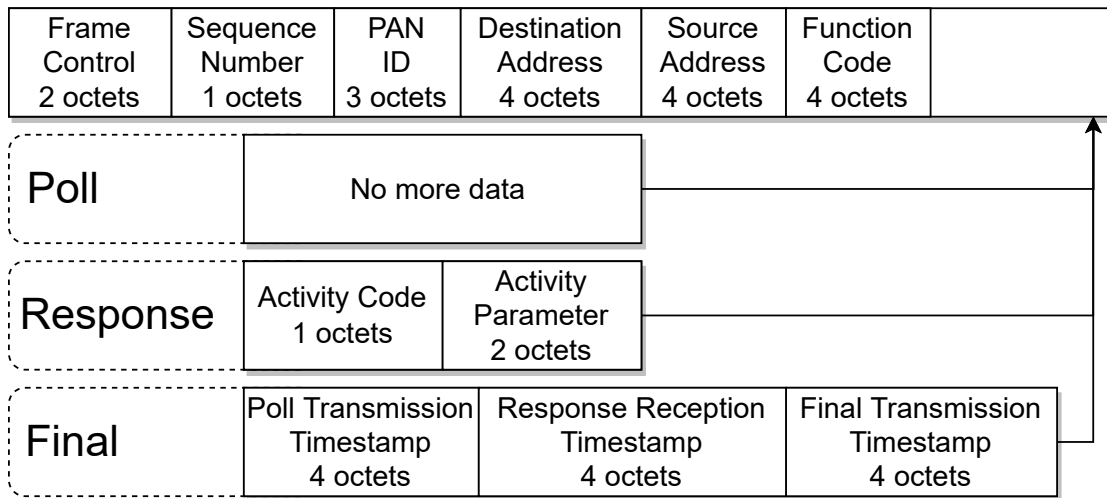


Figure 5.1.: Ultra-wideband packages sent by ranging exchange.

files that are then written contain the date, time, log level and either the azimuth and elevation angle values or the distance value.

To perform a measurement, first start both the BLE and UWB parser with no timing pressure. Then execute the `ex1-main-just-vicon.py` program from Niculescu while pressing the button combination CTRL + ALT + J to activate the BLE and UWB parsers.

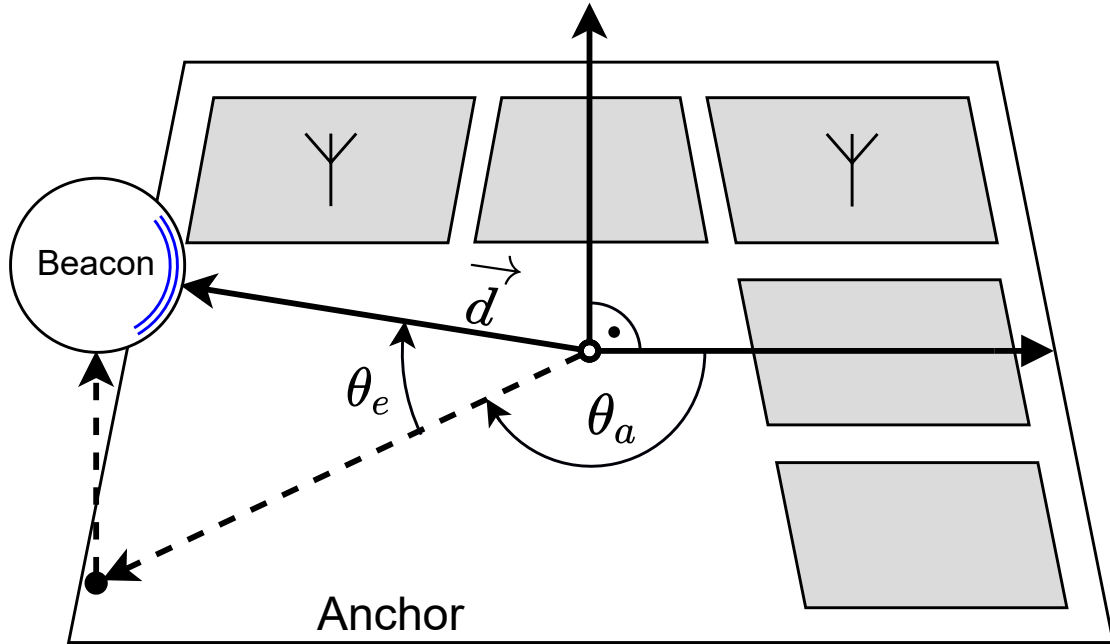


Figure 5.2.: Azimuth, elevation angles and distance vector in relation to center of anchor.

## 5.4. Fusion Of AoA And Distance Data Algorithm

This section discusses the localisation approach of using the angles of arrival and distance measurements obtained by BLE and UWB respectively. Only one anchor with AoA and UWB ranging is needed to localise a beacon for this localisation approach. The location of this anchor is referred to as origin of the world coordinate system and is expected to hang upside down from the ceiling. Figure 5.2 shows the two dimensional equivalents of this system. The beacon would rest on the ground with the azimuth, elevation angles and distance vector marked.

### 5.4.1. Coordinate Transformations

Since our ground truth system is in Cartesian coordinates and our anchor system in polar coordinates, transformations are needed to compare the data.

#### Cartesian to Polar

With equation 5.1 the distance value from  $\vec{d}$  is calculated from the Cartesian coordinates of the anchor and beacon. The anchor coordinates have the subscript  $x_a$  while the beacon has  $x_b$ .

## 5. Firmware Of Beacon And Anchor

$$|\vec{d}| = \sqrt{(x_a - x_b)^2 + (y_a - y_b)^2 + (z_a - z_b)^2} \quad (5.1)$$

With equation 5.2 the azimuth angle  $\theta_a$  can be calculated from the Cartesian coordinates of the anchor and beacon. The calculated angle has the origin at the anchor center. The azimuth angle is in the range of -180 to 180 degrees.

$$\theta_a = \arctan \frac{y_b - y_a}{x_b - x_a} \quad (5.2)$$

With equation 5.3 the elevation angle  $\theta_e$  can be calculated from the Cartesian coordinates of the anchor and beacon. The calculated angle has the origin at the anchor center. The elevation angle is in the range of -90 to 90 degrees.

$$\theta_e = \arctan \frac{z_a - z_b}{(x_a - x_b)^2 + (y_a - y_b)^2} \quad (5.3)$$

### Polar to Cartesian

With equation 5.4 the Cartesian coordinates can be calculated from the polar coordinates. Since the anchor is in reversed position on the ceiling a positive elevation corresponds to a negative z axis. Note that these calculated coordinates will have the anchor location as the world origin point. Thus these coordinates need to be shifted by the anchor locations compared to the ground truth origin.

$$\begin{bmatrix} x \\ y \\ z \end{bmatrix} = \begin{bmatrix} d \cdot \cos \theta_a \cdot \cos \theta_e \\ d \cdot \sin \theta_a \cdot \cos \theta_e \\ -d \cdot \sin \theta_e \end{bmatrix} + \begin{bmatrix} x_a \\ y_a \\ z_a \end{bmatrix} \quad (5.4)$$

To calculate the error that a degree offset  $\theta_N$  creates at a distance of  $d$  we calculate the chord length  $C_{Error}$  of a circle with equation 5.5.

$$C_{Error} = 2d \cdot \sin(\theta_N/2) \quad (5.5)$$



# Chapter 6

## Experimental Setup

In this chapter, the setup of all experiments is introduced with the definition of the ground truth corresponding object tracking. If a file in this chapter is named and not explicitly told otherwise, one can find it in the enclosed git in the appendix C.z

### 6.1. Definition Of Ground Truth - Vicon

Inside the test room, a Vicon motion camera system is mounted, which is used to determine the ground truth for our experiments. The setup consists of six Vicon Vero v2.2 infrared cameras with a resolution of  $2048 \cdot 1088$  pixels, a framerate of 330 Hz, and multiple infrared lamps. These cameras are connected via power over Ethernet enabled Ethernet cables to a Windows machine running the Tracker 3.7.0 software included with the Vicon system. These cameras send out infrared light from around the lens into their field of view. One can utilise little highly reflective balls, which the camera will be able to locate on its two-dimensional picture field. One can thus distinctly triangulate the reflective ball in 3D space with three cameras. All six cameras face the centre reflective point of the room and create a hot zone where any point can be tracked, even if obstacles obstruct some camera vision. The Vicon system guarantees a sub-millimetre precision for this room size and will thus be used as our ground truth to compare our experimental values.

#### 6.1.1. Room Setup For Measurements

Figure 6.1 shows a top-down illustration where the origin point is set at the anchor location in the middle of the room at ground height. The coordinate system direction is marked in the middle of the illustration, with the z-direction pointing upwards. The

## 6. Experimental Setup

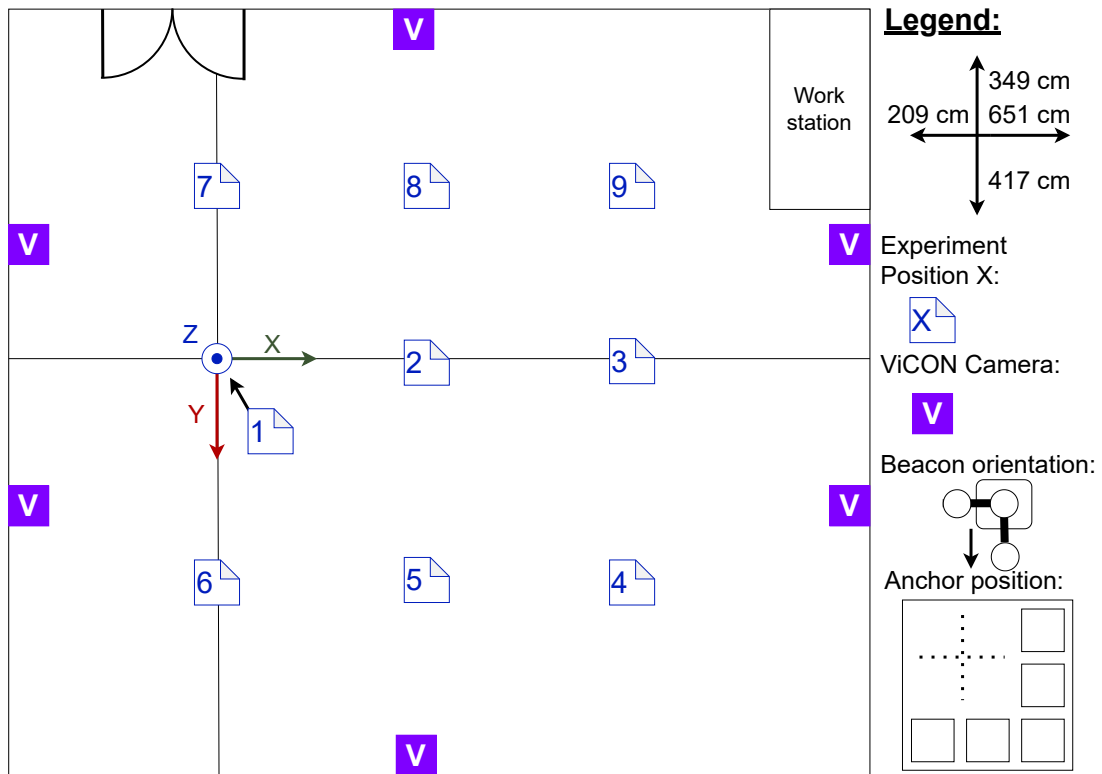


Figure 6.1.: Floorplan of the test room with world coordinate origin at the middle of the room on floor level below where the anchor is located.

approximate location of the Vicon cameras is illustrated in purple, and the Vicon Station is located in the bottom left corner. All of the measurements for this room were measured by hand with a tape measure with a total length of 3 meters, and the corresponding measurements are displayed in table 6.1.

### 6.1.2. Setup Of Vicon System

The Tracker software is installed on a Windows machine, and the cameras are calibrated automatically with a Vicon Active Wand by generating 3000 confirmed sample points on the wand per camera. One needs to move through the whole hot zone during the calibration process until all cameras take on a blue LED colour to signify completed calibration.

To then define the world coordinate system, one can use the Vicon Active Wand again by placing the central LED on the preferred origin point and the outer arms of the wand

## 6. Experimental Setup

Test room depth direction	Value
+ x	(651 $\pm$ 2 cm)
- x	(209 $\pm$ 2 cm)
+ y	(417 $\pm$ 2 cm)
- y	(349 $\pm$ 2 cm)

Table 6.1.: Test room dimensions measured outwards from floor level under anchor location.

in desired positive x and the y-axis direction. The z-axis will be projected in the LED light direction, in essence, to the room's ceiling.

### 6.1.3. Setup Of Anchor

We had two different setup locations for the anchor. The first location was in the centre of the ceiling of the measurement room. The second one got moved along the negative x-axis visible in figure 6.1 to cover the whole hot zone of the Vicon system within  $\pm 90$  degrees of the azimuth angle. The setup location for the anchor was such that the negative x-direction for the Vicon room was small since the u-blox system can only output an azimuth angle of  $\pm 90$  degrees where 0 deg azimuth is aligned with the x-axis. The y axis got divided in half, and thus the anchor was placed in the middle left part of the room, as visible in figure 6.1. The anchor gets attached to two ceiling lights via some carton boxes and the 3D printed mounting case designed in a previous work by Hunziker et al. [30]. The C211 and custom anchor board then get wired via USB cable to the workstation in preparation for the two serial signals. Lastly, three reflective balls are placed at varying heights on the case to make the anchor node visible for the cameras and thus ultimately create our origin point for the calculations. It is necessary to use three distinct points otherwise no trackable object can be created in the Vicon software package. The mounting setup can be seen in figure 6.2.

### 6.1.4. Setup of Beacon

As the test object, the beacon gets put in the case of the C209 U-Blox board and fitted with a battery to improve the ease of testing. On the case, we attached three reflective balls with the ball on the case itself defined as the origin and the other two protruding at a 90-degree angle as shown in figure 6.3. Care was taken to always have the beacon in the same orientation towards the anchor. The orientation is marked with an arrow towards the anchor in the legend to figure 6.1.

## 6. Experimental Setup



Figure 6.2.: Anchor mount for the experiment.



Figure 6.3.: The custom beacon board is encased in the C209 case and prepared for the Vicon system.

### 6.2. Central Static Measurements

The central static measurement is performed with the anchor object on the ceiling, as noted in subsection 6.1.3, at about 208cm height compared to the z-axis origin of the Vicon room. The beacon stays at a fixed location for each measurement period while the angle of arrival and distance is measured by the anchor and logged via serial connection to the host PC. In total 1000 measurements are taken per batch of both UWB and BLE. Each batch is measured at nine different locations visible in figure 6.1 and at two different heights further called *low* at about 37 cm and *high* at 107 cm. Concurrently the location is recorded by the Vicon system and also logged by the Vicon python wrapper.

### 6.3. Dynamic Measurement

To evaluate the performance of a moving beacon, we placed the beacon on top of a carton tower at the high position. After the measurement started, we moved the beacon around the hot zone for 30 seconds in a circular motion and additionally recorded the corresponding timestamps for line-up purposes. Care was taken to position the moving beacon in the same orientation towards the anchor as visible in figure 6.1. The Beacon performed exchanges at a rate of 40 Hz for BLE and 60 Hz for UWB.

# Chapter 7

## Results

In this chapter, results are displayed that will be further touched upon in the discussion in chapter 8. For every result of all measurement the plots are shown in appendix F.

### 7.0.1. Results For Central Static Measurements

We average the Vicon data over time to eliminate measurement outliers since both objects are stationary and thus create our ground truth for this experiment. Depending on the plots, the data gets converted to polar or Cartesian coordinate systems. For the Cartesian plot, we additionally shift the measurement data by the offset of the anchor from the origin. We thus centre the data around the actual anchor location. The following histographic and scatter plots are created by using [data\\_analyzer.ipynb](#) and will be discussed in chapter 8, plots from all other measurements are displayed in appendix F for completeness.

### 7.0.2. Experiment Location #2 Low

In this measurement, the beacon module was placed at low height at experiment position two, corresponding to a positive x position. From the histograms in figure 7.1 one can see that the precision of all three measured polar dimensions is high, given the standard deviation  $\sigma$  of the distance to only being 1.54 cm and  $\sigma$  of both angles being at 1.22 and 1.13 degrees respectively. The deltas between ground truth represented in orange and median in red are in the same way relatively small with 2.33cm, 1.1 and 1.5 degrees. 1.5 degrees corresponds to a circle chord or angle error of about 6.4 cm.

## 7. Results

From the floor plan scatter graph in figure 7.2 one can thus deduce the high precision of the localisation for this experiment for all Cartesian coordinates. Note in green the ground truth location of the anchor and orange the ground truth location of the beacon both measured by the vicon system.

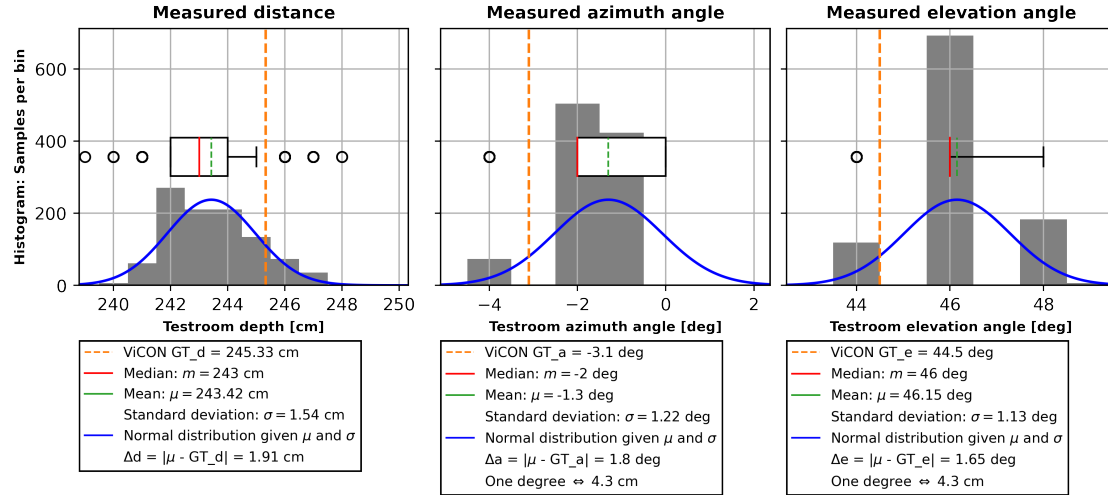


Figure 7.1.: Distance, azimuth and elevation histogram and distribution plots.

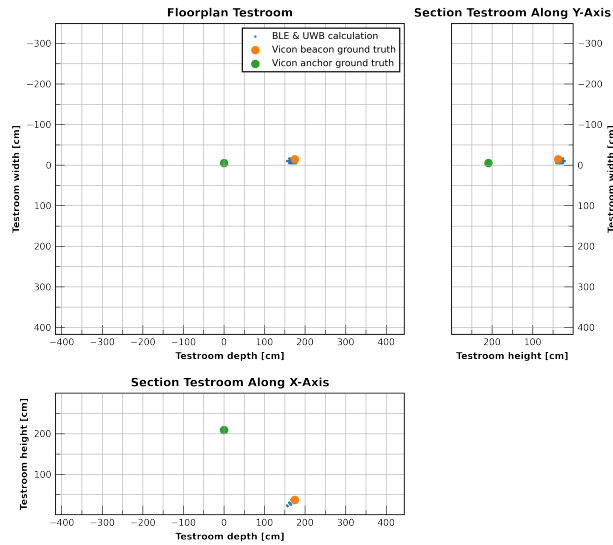


Figure 7.2.: The floor plan and side view of the measurement area. The coordinates for each plot are x/y, z/y, x/z

## 7. Results

### 7.0.3. Experiment Location #2 Low, Setup Moved -X Direction

To see if the position of the anchor and beacon in relation to the Vicon room influenced the measurement data we moved both the anchor and beacon in negative X-direction and repeated the measurement. In figure 7.4 and 7.3 we can see a diverging elevation angle. To see if this change happens randomly or over time we created figure 7.5 to inspect this possibility.

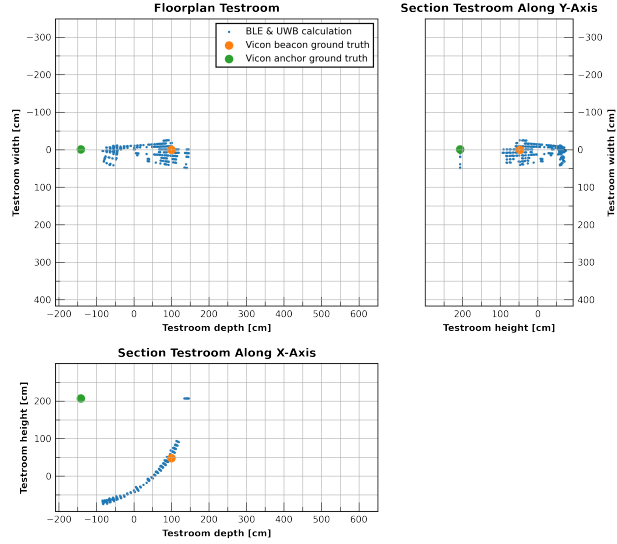


Figure 7.3.: The floor plan and side view of the measurement area. The coordinates for each plot are x/y, z/y, x/z

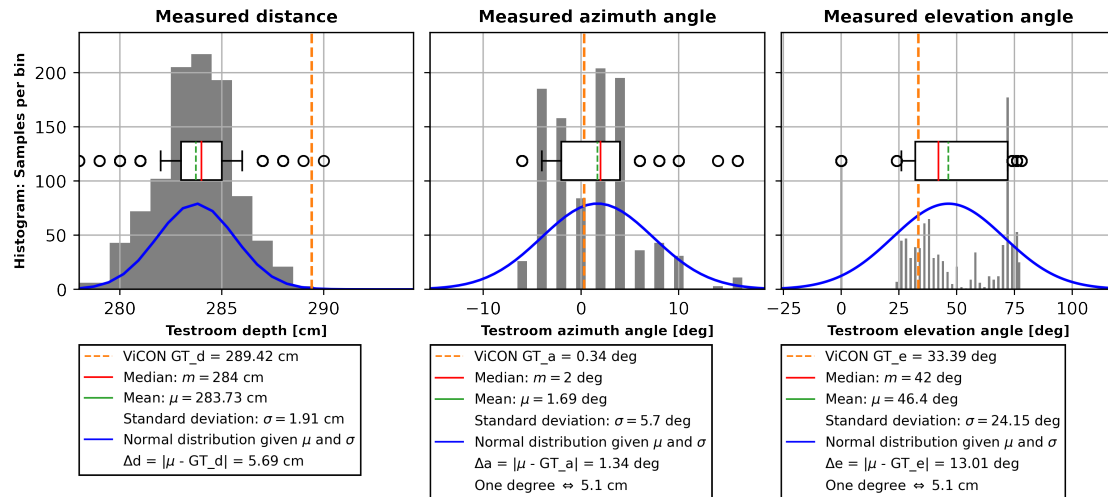


Figure 7.4.: Distance, azimuth and elevation histogram and distribution plots.

## 7. Results

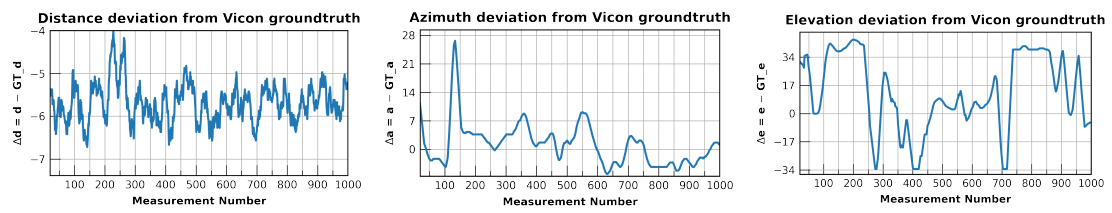


Figure 7.5.: Change of distance, azimuth and elevation delta over measurements taken.



## 7. Results

### 7.0.4. Experiment Location #9 High

Experiment at location 9 and high height shows in figure 7.7 also great standard deviations between all measured axis yet the azimuth and elevation angles have significant deltas between their ground truth and mean. This fact is also visible in figure 7.6 where the presumed beacon location is on ground level yet the beacon is one meter higher.

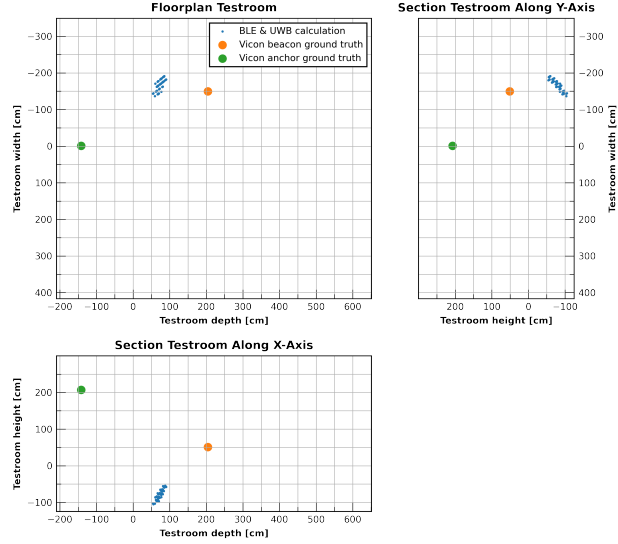


Figure 7.6.: The floor plan and side view of the measurement area. The coordinates for each plot are  $x/y$ ,  $z/y$ ,  $x/z$

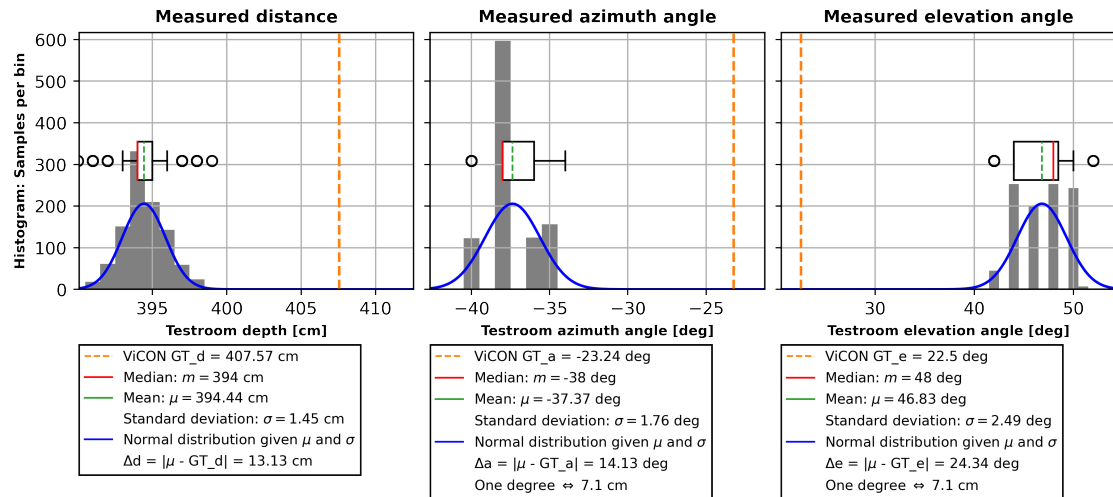


Figure 7.7.: Distance, azimuth and elevation histogram and distribution plots.

## 7. Results

### 7.0.5. Experiment Location #6 Low

From the measurements in figure 7.9 for experiment location six at low height level which is just on the edge of the  $\pm 90$  azimuth degrees possible. We can see the same small standard deviation  $\sigma$  for distance and azimuth angle at 1.89 cm and 1.74 degrees. Yet the elevation angle has a large standard deviation of 10.56 degrees where the 1000 measurements seem to split into two distinct groups at  $+10$  and  $-20$  degrees. This behaviour is also apparent in figure 7.8 where two distinct clouds are formed by the measurements visible in both side view subplots. Additionally, it is visible that the azimuth angle has a significant delta between the ground truth and its median.

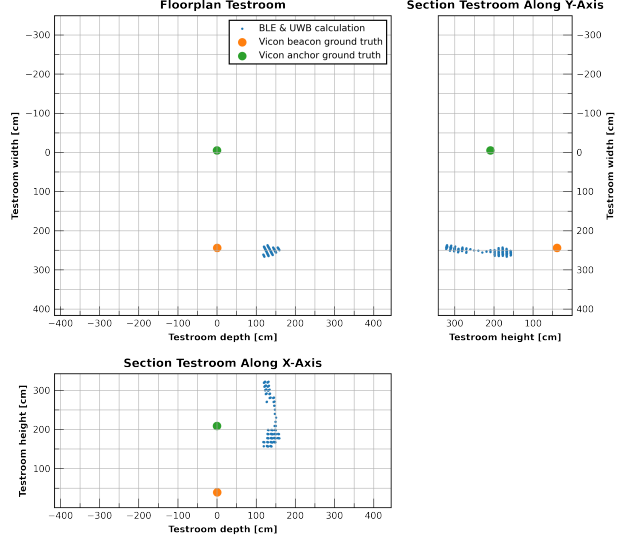


Figure 7.8.: The floor plan and side view of the measurement area. The coordinates for each plot are x/y, z/y, x/z

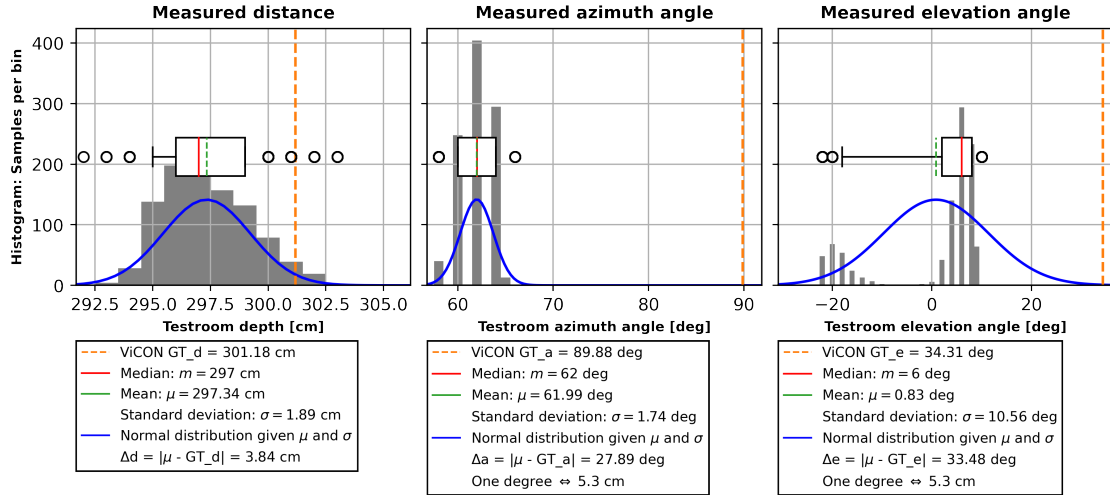


Figure 7.9.: Distance, azimuth and elevation histogram and distribution plots.

## 7. Results

### 7.0.6. Experiment Location #7 Low

The same behaviour is also clearly visible in figure 7.11 of experiment seven at the other end of the  $\pm 90$  degrees azimuth angle range. The same two clusters are visible in figure 7.10 indicated by the high standard deviation of the elevation angle and it is of note that the bigger sample bucket is the one corresponding to a higher position, in essence in the ceiling. Coinciding with this divide the same high delta for the azimuth angle is apparent.

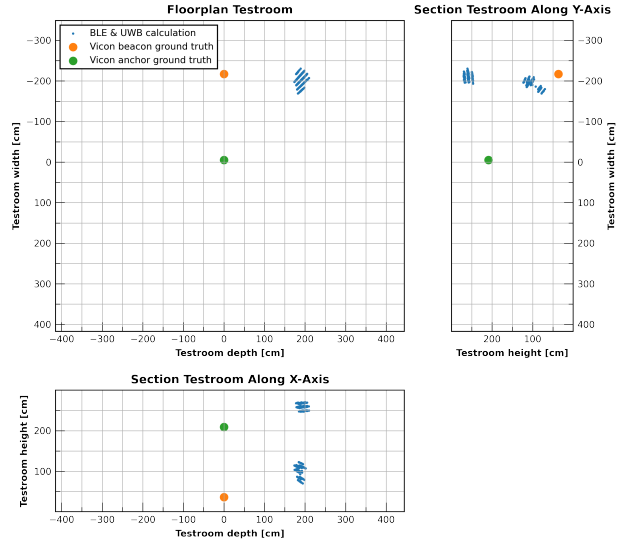


Figure 7.10.: The floor plan and side view of the measurement area. The coordinates for each plot are x/y, z/y, x/z

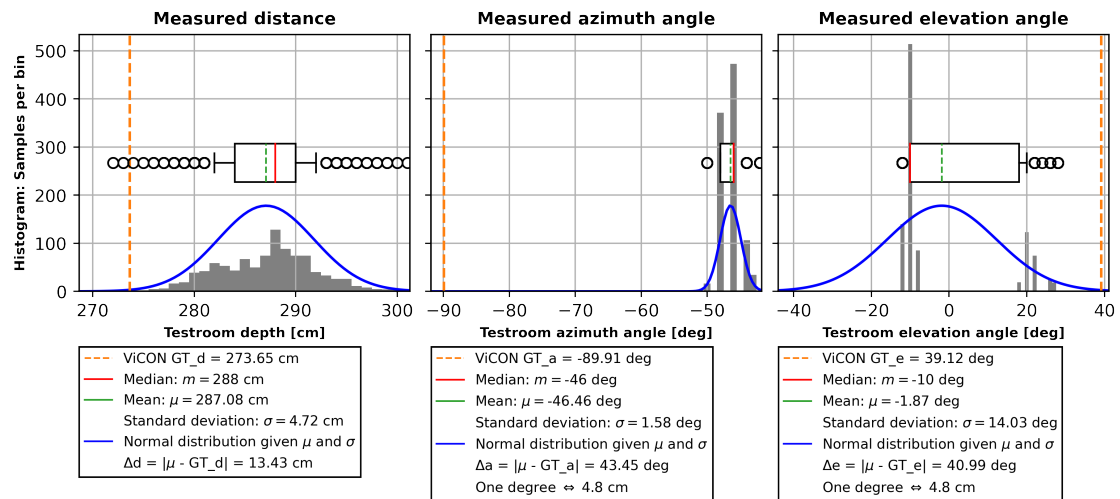


Figure 7.11.: Distance, azimuth and elevation histogram and distribution plots.

## 7. Results

### 7.0.7. Experiment Location #3 High

Lastly, we wanted to highlight an experiment on the high test point at location three. In this experiment, the distance again shows a small delta and deviation. Still, the azimuth and elevation angles have a standard deviation of 20.61 and 29.95 degrees, indicating a complete impossibility to get sufficient confidence as to the beacon's position.

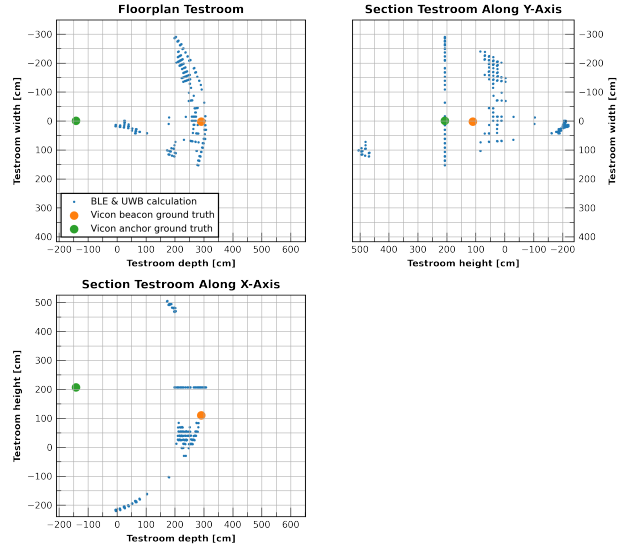


Figure 7.12.: The floor plan and side view of the measurement area. The coordinates for each plot are  $x/y$ ,  $z/y$ ,  $x/z$

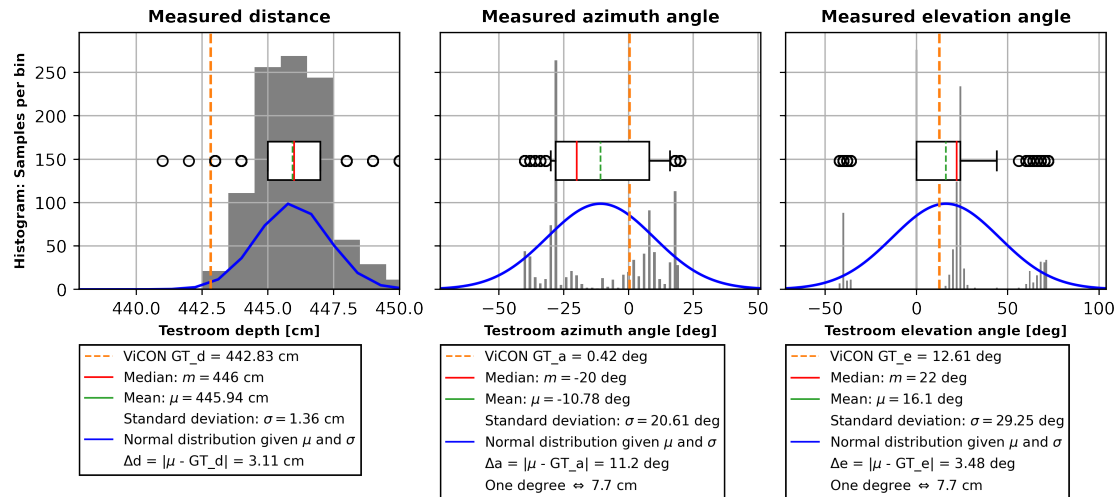


Figure 7.13.: Distance, azimuth and elevation histogram and distribution plots.

## 7. Results

### 7.0.8. Results Dynamic Measurement Circular

In this measurement, we simply moved the beacon in a circular pattern in X/Y space through the hot zone.

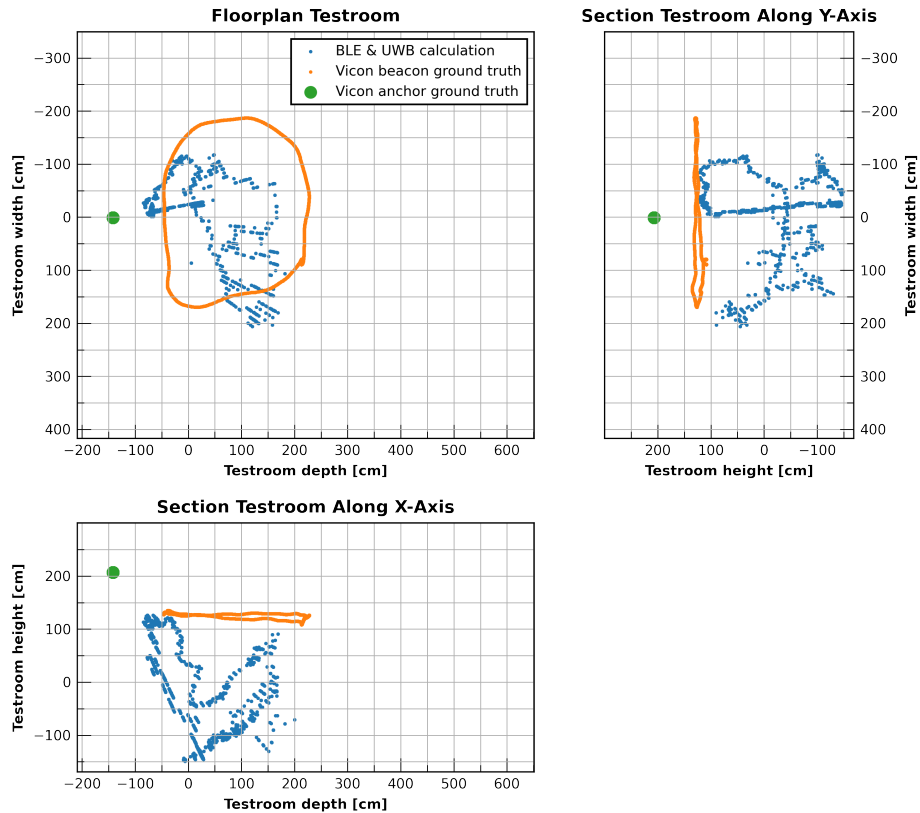


Figure 7.14.: Dynamic circle measurement in Cartesian coordinates.

## 7. Results

### 7.0.9. Results Dynamic Measurement Height

In this measurement, we additionally moved the beacon over different heights around the hot zone.

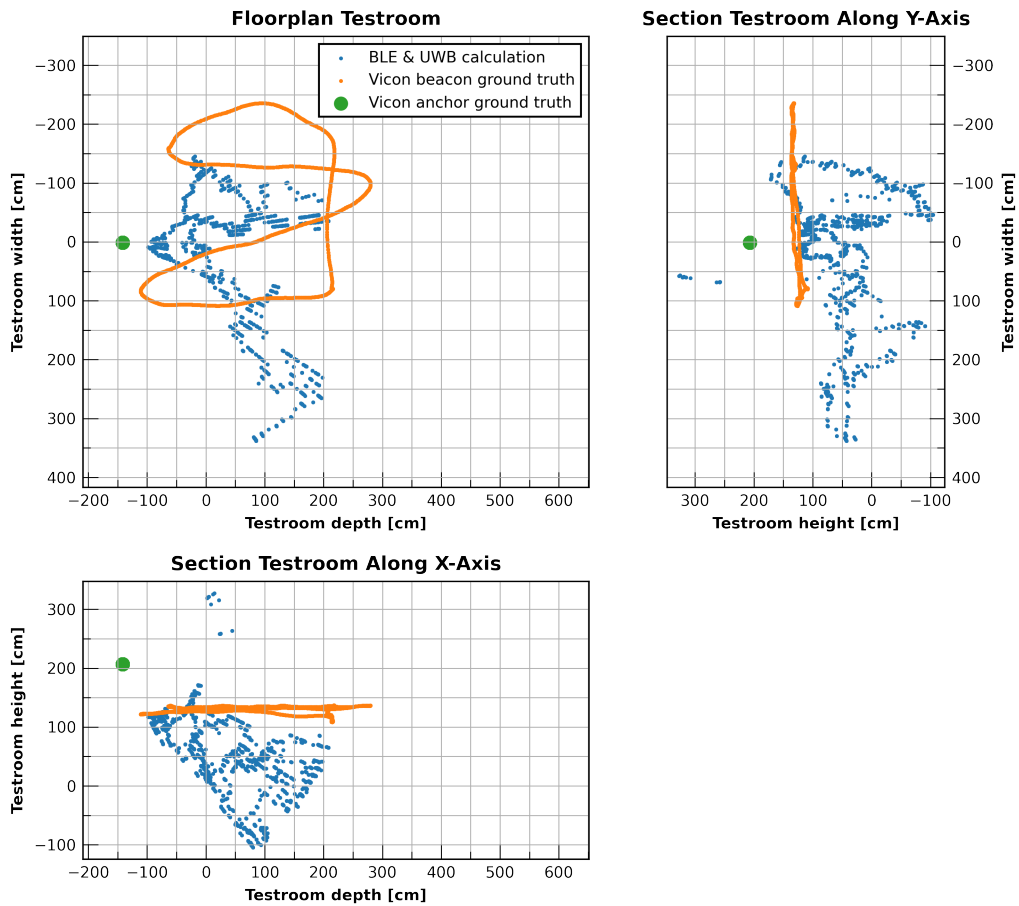


Figure 7.15.: Dynamic height measurement in Cartesian coordinates.

## Discussion

With the results, it is apparent that the UWB ranging performs well. The u-blox AoA system either has a few shortcomings that impede its effectiveness or is downright unusable as a single anchor. In measurement, 7.0.2 the accuracy of all measured axes was satisfactory. Our implementation of the UWB ranging worked as desired, with an offset from the ground truth of 2.33 cm and a standard deviation  $\sigma$  of 1.54 cm over every measurements. At the same time, the angle of arrival system by u-blox allowed us to pinpoint the beacon *in one experiment* by 5.2 cm on average with minimal standard deviation or outliers.

The UWB ranging exchange appears to be relatively indifferent to changes in experiment location with a total average delta  $\Delta_a$  from the ground truth of  $(6.66 \pm 2.16\text{cm})$  with the biggest outlier  $\Delta_a$  being 27.68 cm at close range in experiment one which might indicate a slightly miss calibrated antenna delay. This delta could further be improved with the complete calibration of the antenna delay, which was done to the best of our ability but can be done on a per design basis. The DWM3000, in essence, would need to know the transmission and reception delay incurred due to the circuit design and multiple measurements required to be made at a known length. The total distance was limited by the constraints of the Vicon systems hot zone thus, a maximum of five meters could be measured.

Yet the actual position of the beacon in the test chamber and relative to the anchor appears to have a significant impact on the AoA system. While experiments like 7.0.2 were able to locate the direction of the Bluetooth signal precisely, most examples had either a split data cloud in 3D space with one of the two clouds being correct or were completely off from the ground truth.

The split data clouds from experiments 7.0.5 or 7.0.6 can be explained by a phenomenon called multipath propagation, illustrated in figure 8.1. In this phenomenon, a reflective

## 8. Discussion

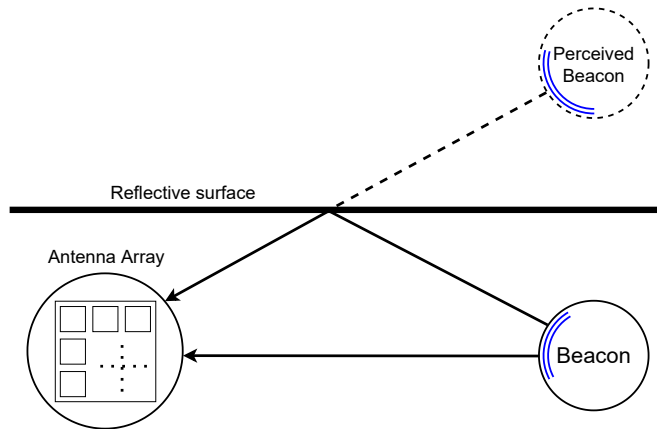


Figure 8.1.: Illustration of multipath propagation.

surface contributes to redirecting a radio signal towards the anchor node. This reflected signal in turn appears to the anchor as a valid origin point and thus gets logged as the position of the beacon. Multipath propagation can not be remedied by removing outliers since the reflective surface will keep redirecting the RF waves. In order to mitigate the multipath propagation, one needs to implement data from other sensors and thus sensor fusion to discern the real origin point. The easiest way is using multiple anchors and thus being able to determine outlier data. This approach of course, is precisely what this work tried to avoid working with. In a next step, one could employ the integrated inertial measurement unit to gather beacon specific forces and transmit those via the UWB ranging packet, thus accumulating more data for the sensor fusion.

These results also show a significant drift in the azimuth angle  $\theta_a$ , which we again explain by multipath propagation. Due to the fact that the no blocking objects were introduced in the experiment, we would at least expect another point cloud on the ground truth position itself in addition to the false data. Since we do not see this represented in real-world data, we envision another culprit, *Rician fading*, which is a byproduct of multipath propagation. In Rician fading, a RF signal arrives at the receiver by several different paths but has one signal that is much stronger than the others, generally the line of sight signal. If no distinctly strong signal is present this effect reduces to the so called Rayleigh fading. In both cases, radio waves take multiple paths from beacon to anchor. At the anchor, these waves give rise to an increase or decrease of amplitude on the measured signal compared to the expected signal if the anchor received only one RF signal. Figure 8.2 shows an illustration of Rician fading where the received signals create a different prediction in comparison to only the line of sight radio signal.



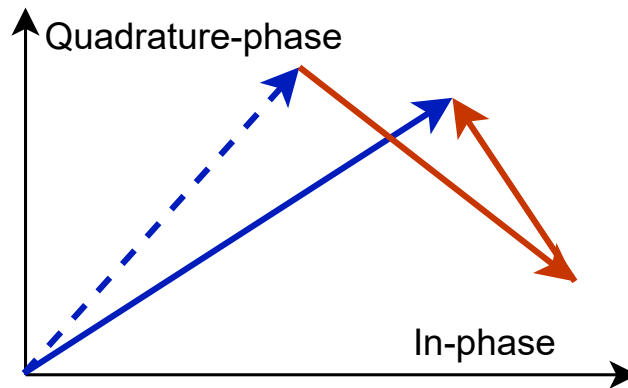


Figure 8.2.: Illustration of impact of reflected waves on the measured signal.  
 Blue dashed line - line of sight direction  
 Red full line - multipath rf signals  
 Blue full line - perceived direction by receiver

For the dynamic measurements, we can not uphold cautious optimism. In all results of 7.0.8 and 7.0.9 there is no resemblance of a coherent path visible that the beacon took. The accuracy is in the range of meters, and the error appears random as seen in the elevation curve over all samples from figure 7.5. The error is at least a combination of all three phenomena discussed in this chapter. With the BLE SAL being in the accuracy range of about two meters at a distance of two to three meters is not meaningful data and would require measurements in a bigger room or warehouse to further distinguish these effects. Thus we have to say that we can not use the BLE angle of arrival anchor from u-blox for single anchor localisation without further changes.

As a final note to get the same decimeter precision as UWB at 50 meters with BLE we would require a general precision of  $\pm 0.1$  to 1 degrees.

Contrasting these findings with related work like Monfared et al. [11] with a 90% precision of 1.8 meters it is apparent that the BLE precision is in the same range as our experiments but in contrast to UWB is just seems so much more imprecise. UWB works like Großwindhager et al. [13] recorded a 90% precision of 50 cm while our biggest outlier was 30 cm for the UWB distance dimension. This of course is only part of the picture since Großwindhager et al. additionally used UWB for AoA. While a maximum distance was not mentioned, with a classical office being 10 meters long at most, their angle error is in the range of  $\pm 1.5$  degrees.

# Chapter 9

## Conclusion

In this work, a single anchor localisation system was constructed consisting of the Bluetooth indoor localisation anchor designed by u-blox and the ultra-wide band antenna designed by Qorvo. It is shown that localisation data can be drawn from a one anchor system. The UWB component showed decimeter accuracy and proved resilient to disturbances. We can not say the same for the proprietary BLE system. While it could sometimes localise devices with reasonable precision and accuracy, that was not always the case. Most of the measurements showed susceptibility to multipath propagation and Rician fading, thus making the data imprecise in a static environment and downright unusable in a dynamic setting. We observed an upper precision of over a meter, a difference of one or two orders of magnitude compared to the UWB sensor.

## 9.1. Future Work

- **Custom BLE AoA Board.** Due to the nature of the proprietary hardware of the u-blox BLE localisation system, we could act on these interference factors by incorporating another RF signal algorithm. Currently, SALMA by Großwindhager et al. [13] looks perfect for this use case. We would like to design our own BLE antenna array with an included UWB chip for future work. A one in all solution.
- **UWB AoA implementation.** With the arrival of the new DW3120 transceivers by Qorvo with integrated ultra-wide band angle of arrival support, this module could also simplify our prototype to only incorporate UWB modules, which would cut down on anchor size. Further advantages and drawbacks still need to be ascertained in future work.
- **Multiple tags.** Due to timing constraints and the need to first gauge the viability of this system, multi-tag support was not implemented. Yet, with the myriad of existing anti-collision schemes for RF, one could rapidly be applied for the UWB solution. The BLE anchor can out of house handle five different beacons. Therefore, a suitable case should be designed for the board and the solar panels.
- **Test in large warehouse.** With the u-blox anchor being rated to a minimum of a two-meter distance, this experimental setup was on the short end of feasibility. To get more real-world data applicable for hospitals or a larger warehouse we would like to conduct further experiments in a bigger setting.

Task Description for a Semester Thesis on

# Fusion of BLE Direction Finding and UWB Ranging for Indoor Localization

at the Departement of Information Technology and  
Electrical Engineering

for

**Nando Galliard**  
gnando@student.ethz.ch

**Advisors:** Silvano Cortesi, silvano.cortesi@pbl.ee.ethz.ch  
**Professor:** Prof. Dr. Luca Benini, lbenini@iis.ee.ethz.ch  
**Handout Date:** 14.02.2022  
**Due Date:** XX.04.2022

## Project Goals

Bluetooth Low Energy (BLE) Direction Finding is a novel technology added to the Bluetooth Specification with the aim to use BLE for Indoor Localization. It specifies an addition to the protocol to support angle of arrival (AoA) as well as angle of departure measurements (AoD). As no reliable distance measurement for BLE is available yet, for a precise localization there is need for at least three anchor nodes with each multiple antenna arrays. Ultra wideband (UWB) is on the other hand a well known protocol used for Indoor Localization using different ranging methods and performing then a trilateration with at least three nodes.

If we are able to combine these two methods on a single anchor, getting angle of arrival as well as distance data, we are able to perform Indoor Localization with a single anchor.

Thus the aim of this thesis is to

- acquire angle of arrival informations using BLE Direction Finding
- acquire distance informations using UWB
- combine the two informations in order to perform a localization
- evaluate the performance of the system

## Tasks

The project will be split into three phases, as described below:

### Phase 1 (Week 1)

1. Investigate the state-of-the-art of the single blocks (BLE Direction Finding, UWB Ranging).
2. Study and get used to the hardware and the tools to program, i.e. microcontroller programming using Zephyr, provided PCB, . . . .
3. The main aim of this phase is to get used to Zephyr and the used technologies.

### Phase 2 (Week 2-3)

1. Integration of the DWM3000 drivers to Zephyr
2. Creating two applications using Zephyr which
  - a) Perform two-ways ranging with an UWB base node
  - b) Advertise an Eddystone beacon containing the constant tone extension for BLE Direction Finding
3. Merge the two applications into a single one

### **Phase 3 (Week 4-5)**

1. Evaluate and characterize the performance of the two measurements separately
2. Implement a simple algorithm to fuse the two measurement data (provided by Silvano Cortesi)
3. Evaluate and characterize the performance of the sensor fused system.

### **Phase 4 (Week 6-7)**

1. Finalize evaluation of the system
2. Writing of the report
3. Creation of the presentation

### **Milestones**

By the end of **Phase 1** the following should be completed:

- Gained knowledge about the used technologies (BLE Direction Finding, UWB Ranging)
- Know how the Zephyr system works and how to use it in order to
  - Create new board files for a custom PCB
  - Add a driver/module to the Zephyr ecosystem
  - Create an (out-of-tree) application using the Zephyr ecosystem

By the end of **Phase 2** the following should be completed:

- The driver for the DWM3000 should be integrated into Zephyr
- A finalized application should be created, providing the tag node with the capabilities for BLE Direction Finding as well as UWB Ranging

By the end of **Phase 3** the following should be completed:

- The UWB Ranging / distance measurement should be evaluated and characterised
- The BLE Direction Finding / angle measurement should be evaluated and characterised
- The combined system should be evaluated and characterised

By the end of **Phase 4** the following should be completed:

- Final design and last in-field tests
- Final report and presentation

## **Project Organization**

### **Weekly Report**

There will be a weekly report sent by the candidate at the end of every week. The main purpose of this report is to document the project's progress and should be used by the student as a way to communicate any problems that arise during the week.

### **Project Plan**

Within the first weeks of the project, you will be asked to prepare a project plan. This plan should identify the tasks to be performed during the project and sets deadlines for those tasks. The prepared plan will be a topic of discussion of the first week's meeting between you and your advisers. Note that the project plan should be updated constantly depending on the project's status.

### **Final Report and Paper**

PDF copies of the report are to be turned in. References will be provided by the supervisors by mail and at the meetings during the whole project.

### **Final Presentation**

There will be a presentation (15 min presentation and 5 min Q&A for BT/ST and 20 min presentation and 10 min Q&A for MT) at the end of this project in order to present your results to a wider audience. The exact date will be determined towards the end of the work.

### **References**

Additional references will be provided by the supervisors by mail and at the meetings during the whole project.



## Declaration of originality

The signed declaration of originality is a component of every semester paper, Bachelor's thesis, Master's thesis and any other degree paper undertaken during the course of studies, including the respective electronic versions.

Lecturers may also require a declaration of originality for other written papers compiled for their courses.

I hereby confirm that I am the sole author of the written work here enclosed and that I have compiled it in my own words. Parts excepted are corrections of form and content by the supervisor.

**Title of work** (in block letters):

FUSION OF BLE DIRECTION FINDING AND UWB RANGING FOR INDOOR LOCALIZATION

**Authored by** (in block letters):

*For papers written by groups the names of all authors are required.*

**Name(s):**

GALLIARD

**First name(s):**

NANDO

With my signature I confirm that

- I have committed none of the forms of plagiarism described in the '[Citation etiquette](#)' information sheet.
- I have documented all methods, data and processes truthfully.
- I have not manipulated any data.
- I have mentioned all persons who were significant facilitators of the work.

I am aware that the work may be screened electronically for plagiarism.

**Place, date**

ZÜRICH, 25/04/22

**Signature(s)**

*For papers written by groups the names of all authors are required. Their signatures collectively guarantee the entire content of the written paper.*



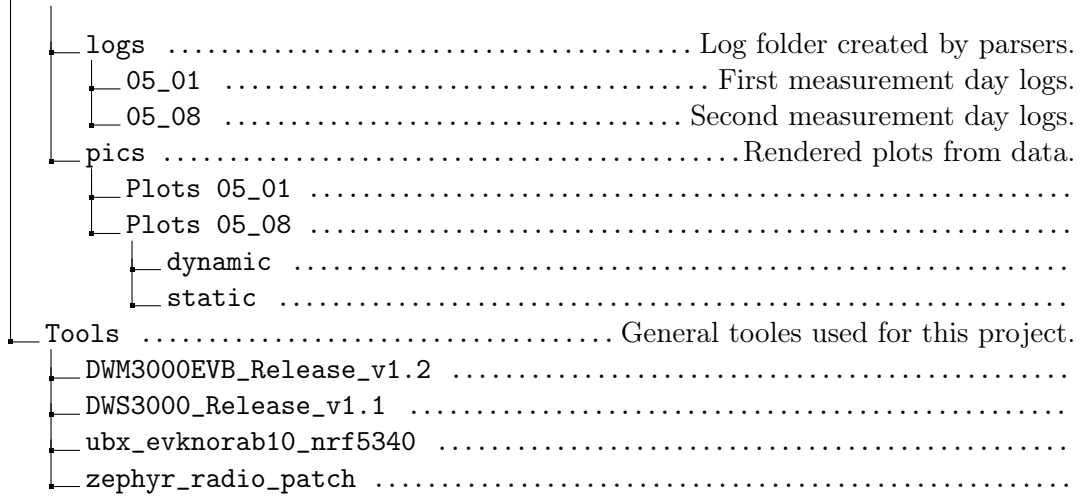
# Appendix C

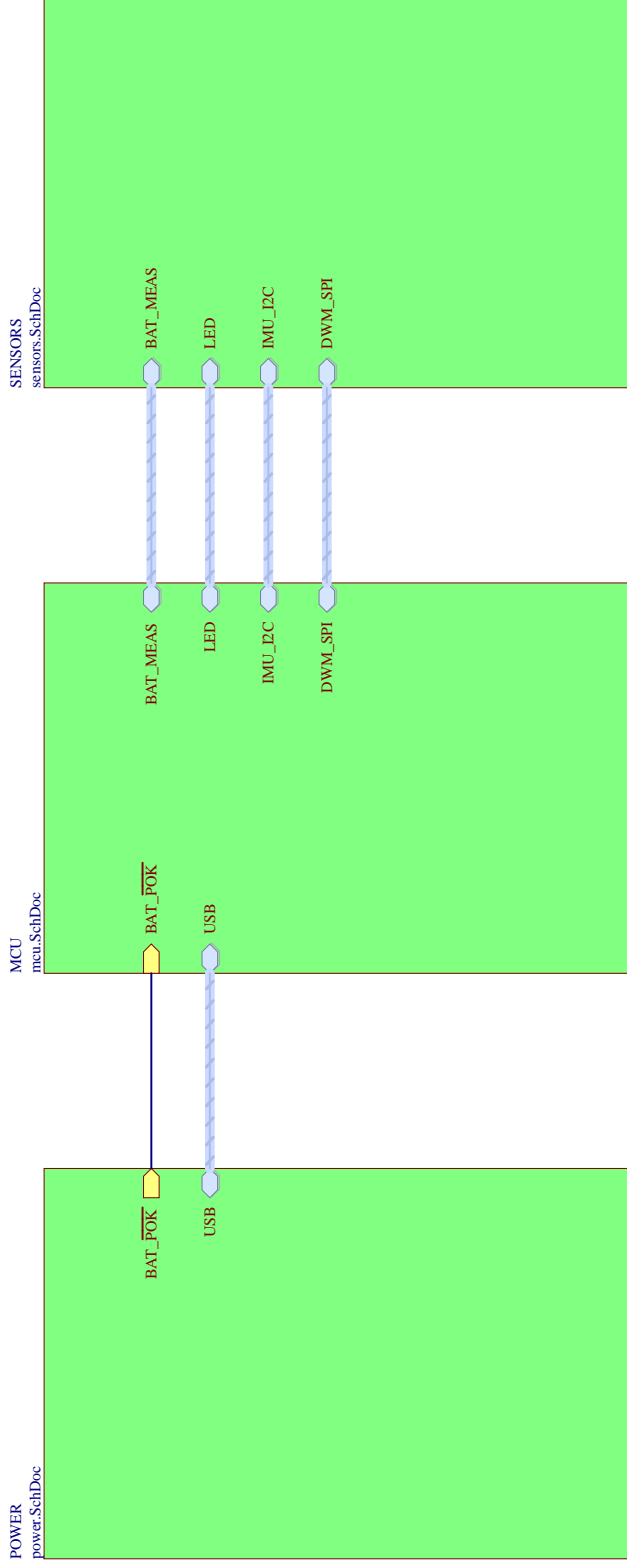
## File Structure

In this chapter we give a overview over the project git directories and files.

Git_SensorFusion	.....
├─ README.md	..... A README with some general information about the project.
├─ Datasheets	..... Multiple datasheets to all relevant components.
├─ Firmware	..... Main folder of the firmware.
│   └─ BLE_and_UWB	.....
│       └─ Anchor_Board	..... Anchor board firmware for UWB.
│       └─ Beacon_Board	..... Beacon board firmware for BLE and UWB.
│   └─ boards	..... Custom board folders.
│       └─ arm	.....
│           └─ ble_uwb_siltag	..... Beacon board files / descriptors.
│       └─ shields	.....
│           └─ qorvo_dwm3000	..... Shield files for the UWB chip.
└─ modules	.....
└─ modules.cmake	..... Adds cmake and Kconfig flags for all modules.
└─ dwm3000	..... UWB driver for version 1.1.
└─ dwm3000_nd	..... UWB driver for version 1.2 - unfinished.
└─ lsm6dsv16	..... IMU driver.
├─ Report	.....
│   └─ Figures	.....
│   └─ Presentation	.....
├─ Software	..... Data handling software.
│   └─ duangulation_plus_lat.ipynb	..... Data handling jupyter notebook.
│   └─ parser.ipynb	.....
│   └─ parser_ble.py	..... Parser for BLE data.
│   └─ parser_uwb.py	..... Parser for UWB data.
│   └─ parser_uwb_average_distance_out.py	.....

### C. File Structure





Eidgenössische Technische Hochschule Zürich  
Swiss Federal Institute of Technology Zurich

Project:

**BLE and UWB Tag**

Drawing number: 1  
Date: 21.10.2021

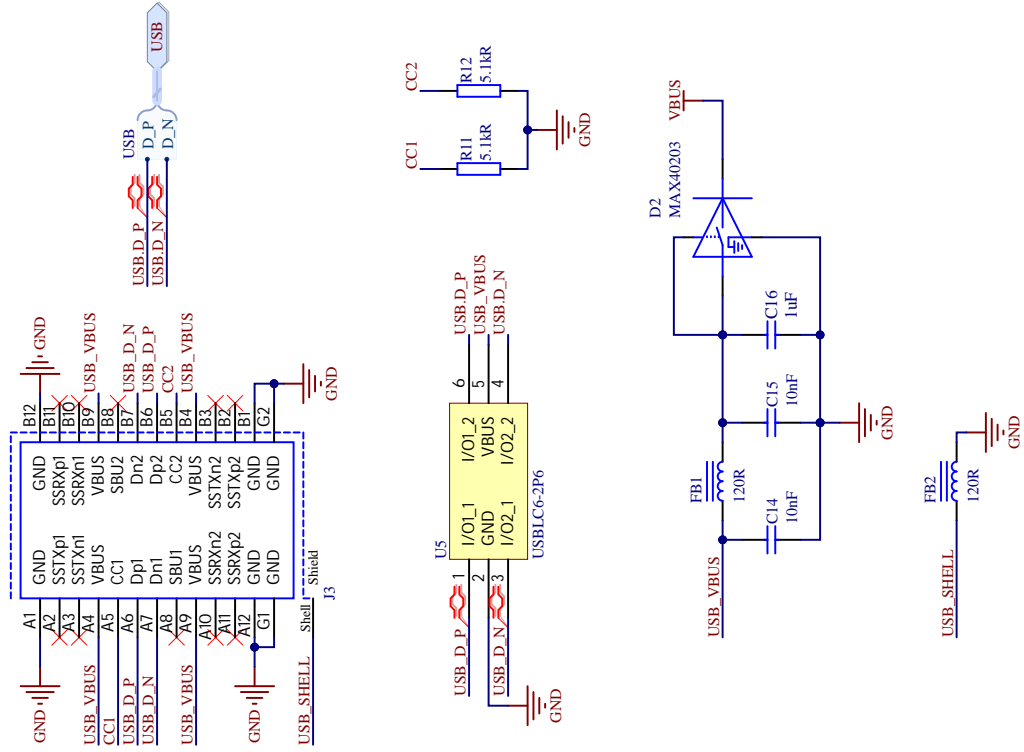
Rev: 1.0  
15:20:20

Format: A4 Q  
Laboratory: Center for Project-Based Learning  
Drawn by: Silvano Cortesi

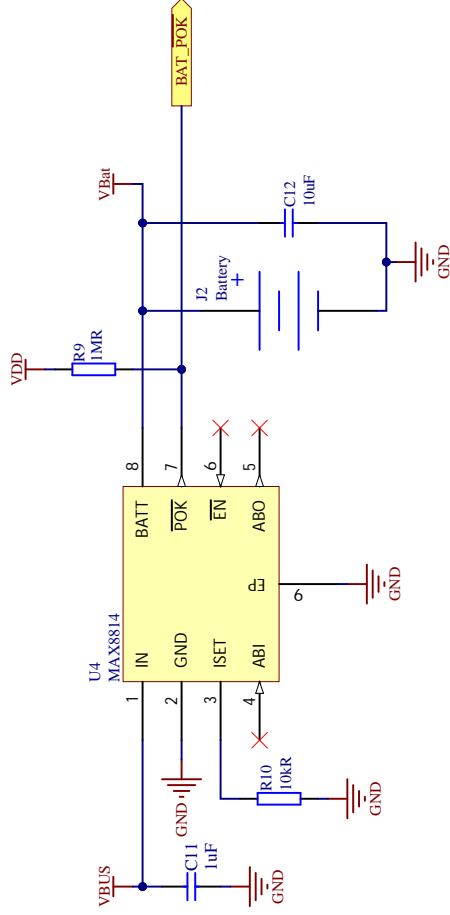
Sheet: main.SchDoc  
Page 1 of 4

File: Y:\Documents\BLE\_UWB\_Board\schematics\main.SchDoc

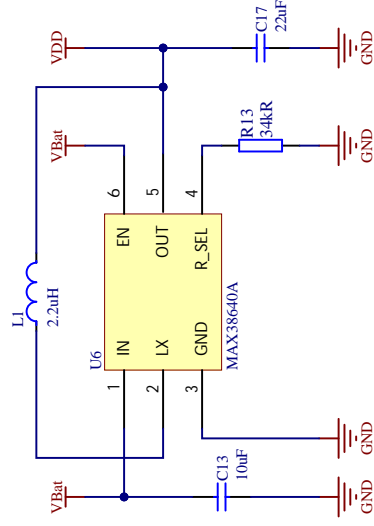
# USB Circuit



# LiPo Charger



# 2.75V Buck Converter



Eidgenössische Technische Hochschule Zürich  
Swiss Federal Institute of Technology Zurich

Project:

BLE and UWB Tag

Drawing number: 2

Rev: 1.0

Format: A4 Q

Laboratory: Center for Project-Based Learning

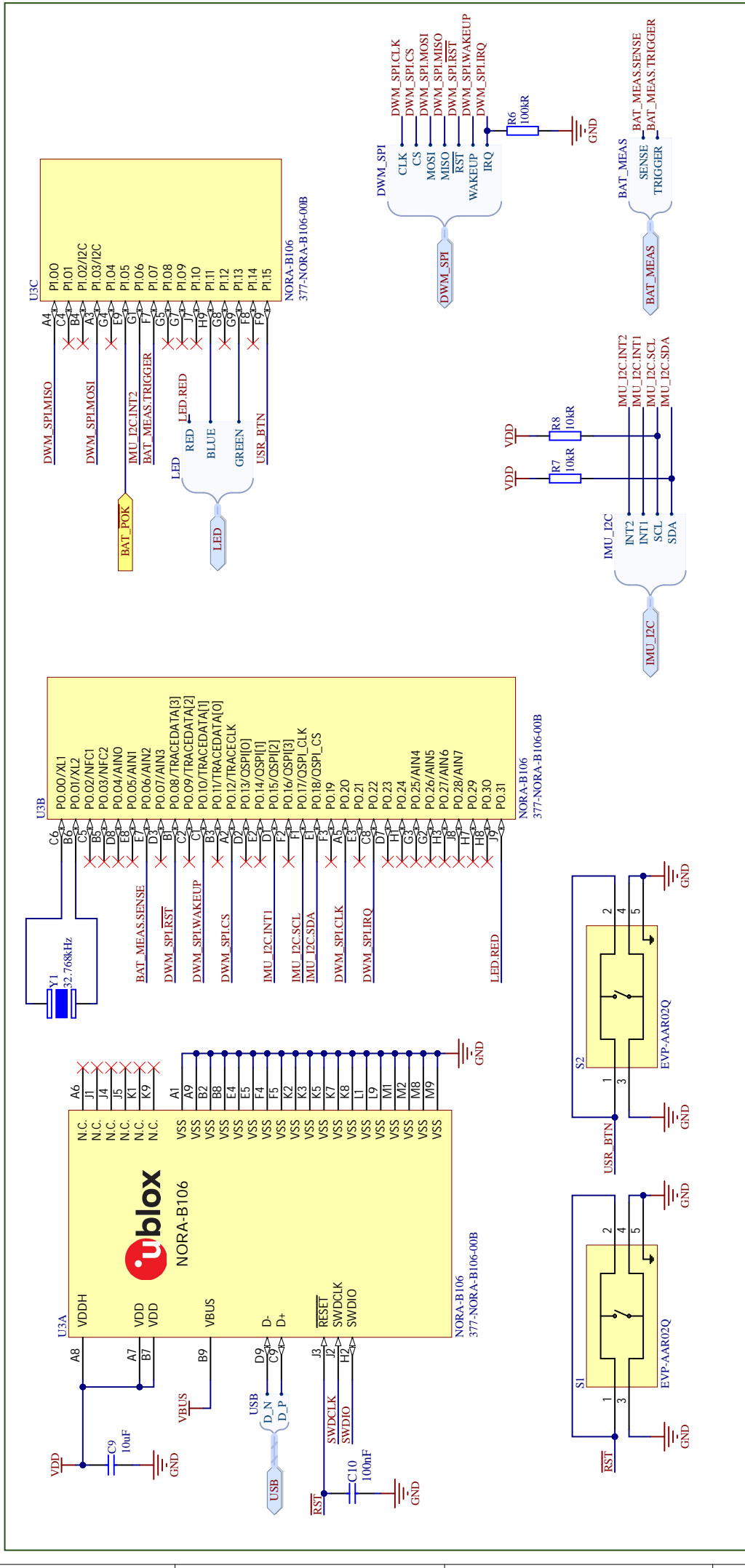
Sheet: power.SchDoc  
Page 2 of 4

Date: 21.10.2021 15:20:20

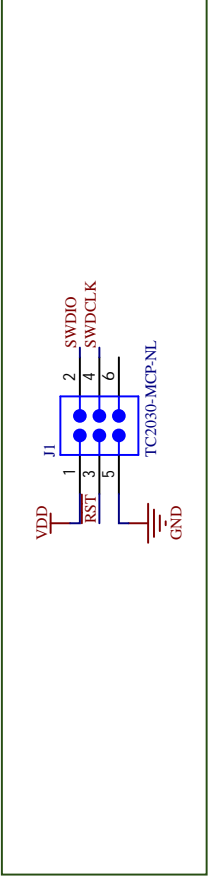
Drawn by: Silvano Cortesi

File: Y:\Documents\BLE\_UWB\_Board\schematics\power.SchDoc

# MCU & BLE



# Programming Connector



Eidgenössische Technische Hochschule Zürich  
Swiss Federal Institute of Technology Zurich

Project:

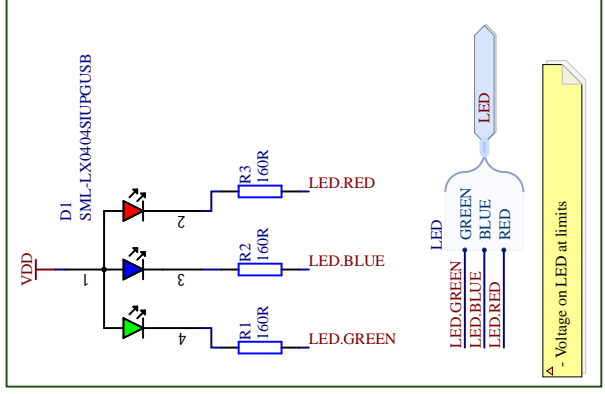
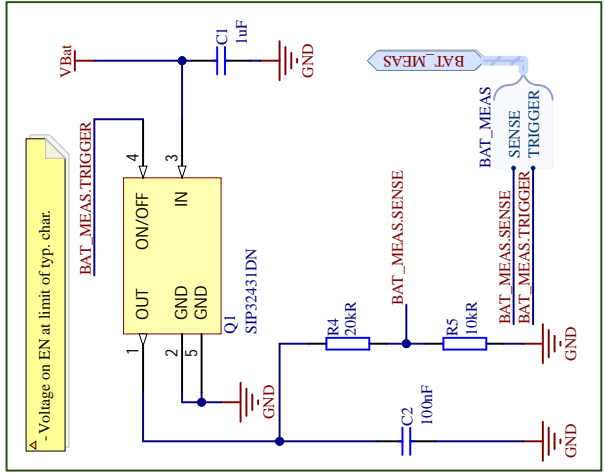
**BLE and UWB Tag**

Drawing number: 3 Rev: 1.0  
Date: 21.10.2021 15:20:20  
File: Y:\Documents\BLE\_UWB\_Board\schematics\mcpu.SchDoc

Format: A4 Q  
Laboratory: Center for Project-Based Learning  
Drawn by: Silvano Cortesi

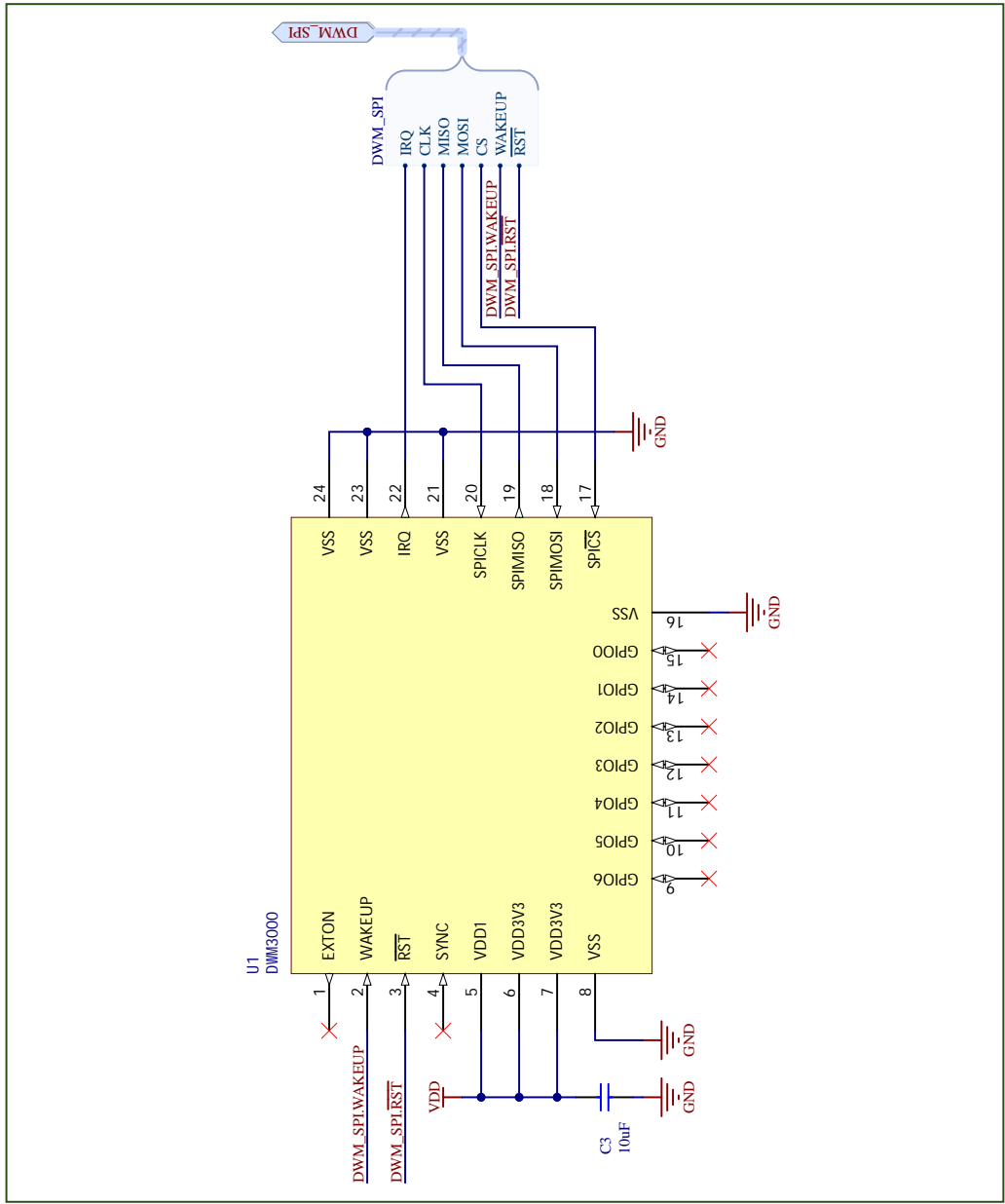
Sheet: mcpu.SchDoc  
Page 3 of 4

### Battery Monitor

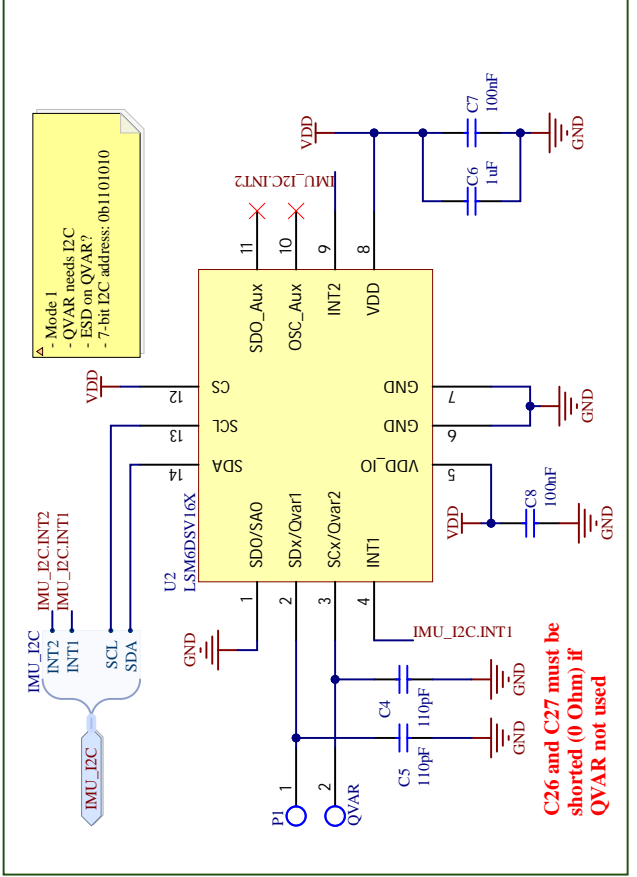


### RGB LED

### Ultra-Wide Band



### IMU



Eidgenössische Technische Hochschule Zürich  
Swiss Federal Institute of Technology Zurich

Project:

BLE and UWB Tag

Drawing number: 4  
Date: 21.10.2021 15:20:21

Format: A4 Q  
Laboratory: Center for Project-Based Learning  
Drawn by: Silvano Cortesi

Sheet: sensors.SchDoc  
Page 4 of 4

File: Y:\Documents\BLE\_UWB\_Board\schematics\sensors.SchDoc

# Appendix **E**

## Zephyr Code Appendix

### E.1. Application

CMakeList.txt

```
1 cmake_minimum_required(VERSION X.XX.X)
2 list(APPEND ZEPHYR_EXTRA_MODULES
3   $ENV{PROJECT_ROOT}/modules/foobar
4   )
5 list(APPEND BOARD_ROOT $ENV{PROJECT_ROOT})
6 set(BOARD foo)
7 set(SHIELD egg_bar)
8
9 include($ENV{ZEPHYR_BASE}/cmake/app/boilerplate.cmake NO_POLICY_SCOPE)
10 project(app)
11 target_sources(app PRIVATE main.c)
12 target_include_directories(app PRIVATE .)
```

### E.2. Modules

CMakeList.txt

```
1 zephyr_include_directories(
2   driver
3   )
4 zephyr_library()
5 zephyr_library_sources(
```

## E. Zephyr Code Appendix

```
6     driver/driver.c
7 )
```

### module.yml

```
1 name:
2   foobar
3 build:
4   cmake: zephyr
5   kconfig: zephyr/Kconfig
6   settings:
7     dts_root: zephyr
```

### modules.cmake

```
1 set(ZEPHYR_FOOBAR_CMAKE_DIR ${CMAKE_CURRENT_LIST_DIR}/foobar/zephyr)
2 set(ZEPHYR_FOOBAR_KCONFIG   ${CMAKE_CURRENT_LIST_DIR}/foobar/zephyr/Kconfig)
```

Check if this can be left out?



# Appendix F

## Remaining Plots

Find all measurements in this chapter. If a measurement position is noted refer to figure 6.1 for the illustration of the Vicon room and the corresponding positions.

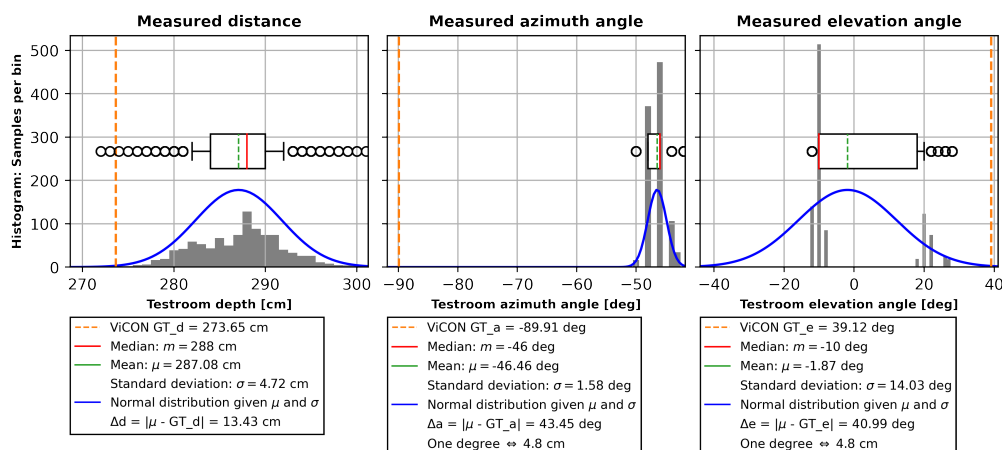


Figure F.9.: 01 Mai Experiment  
Position 7 Histogram Plot

F. Remaining Plots

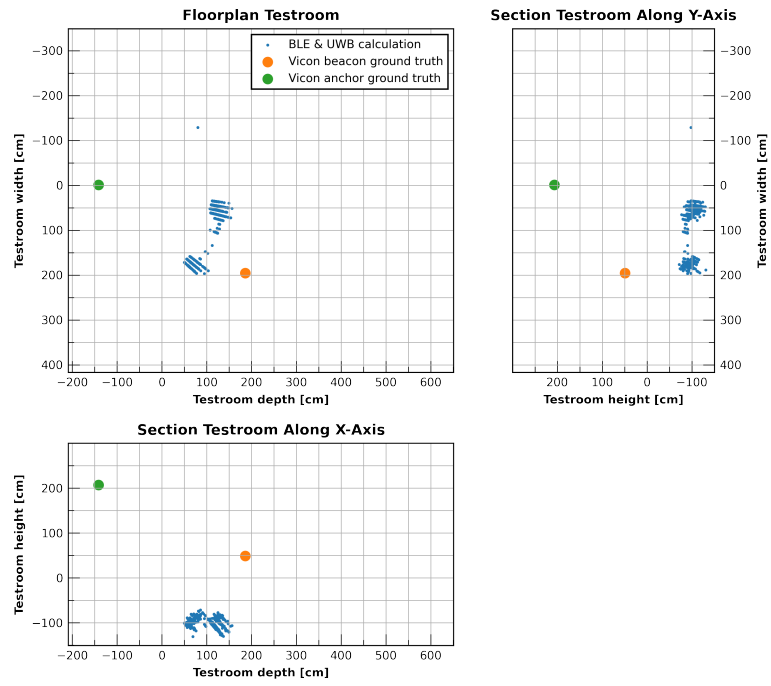


Figure F.10.: 01 Mai Experiment  
Position 2 Position Plot

## F. Remaining Plots

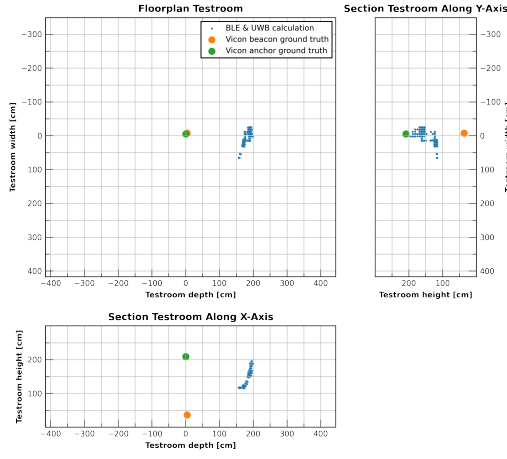


Figure F.1.: 01 Mai Experiment  
Position 1 Position Plot

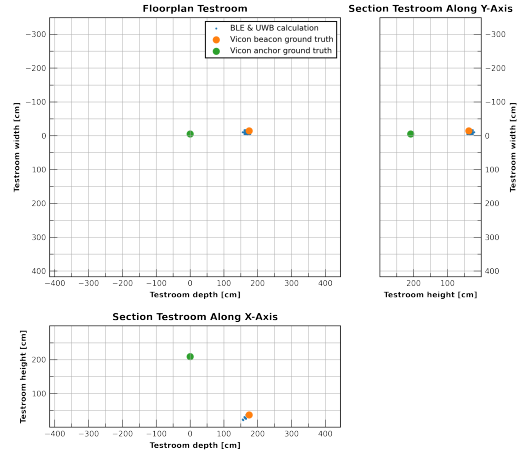


Figure F.2.: 01 Mai Experiment  
Position 2 Position Plot

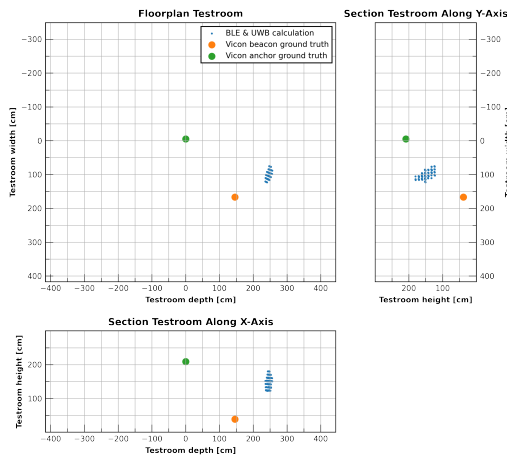


Figure F.3.: 01 Mai Experiment  
Position 5 Position Plot

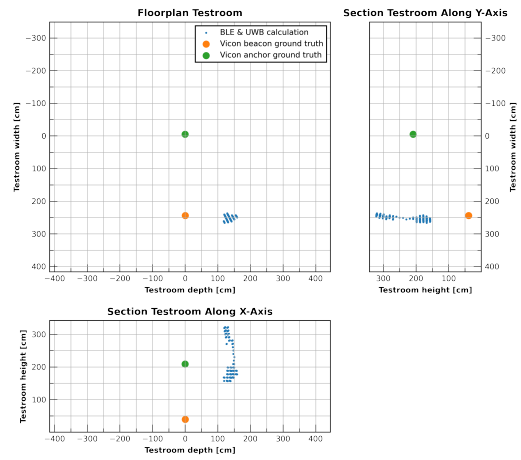


Figure F.4.: 01 Mai Experiment  
Position 6 Position Plot

## F. Remaining Plots

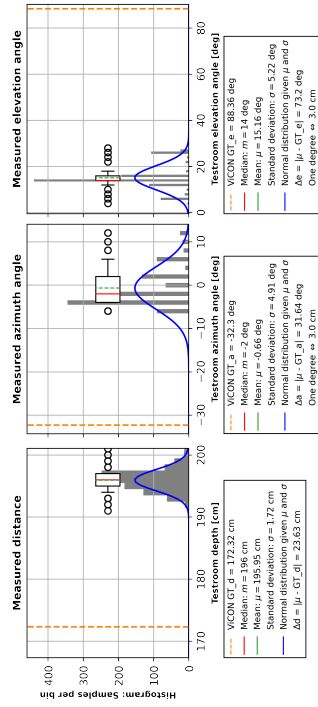


Figure F.5.: 01 Mai Experiment  
Position 1 Histogram Plot

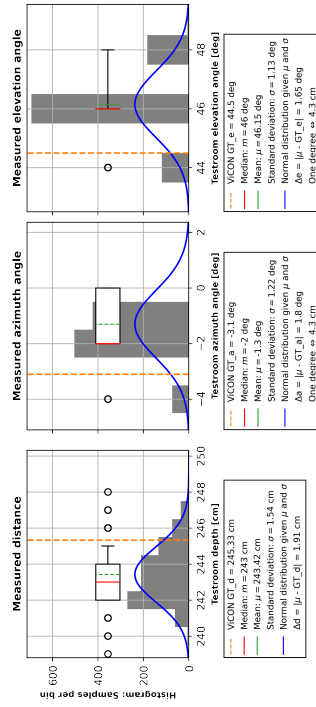


Figure F.6.: 01 Mai Experiment  
Position 2 Histogram Plot

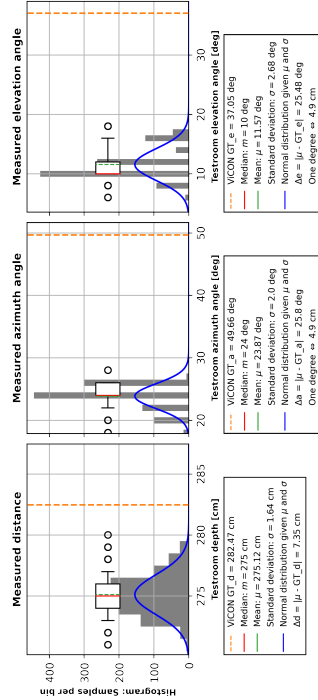


Figure F.7.: 01 Mai Experiment  
Position 5 Histogram Plot

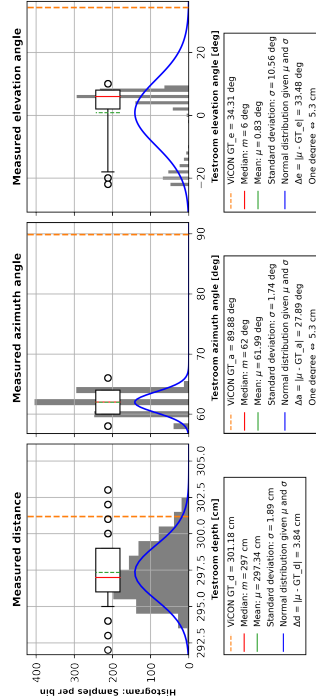


Figure F.8.: 01 Mai Experiment  
Position 6 Histogram Plot

## F. Remaining Plots

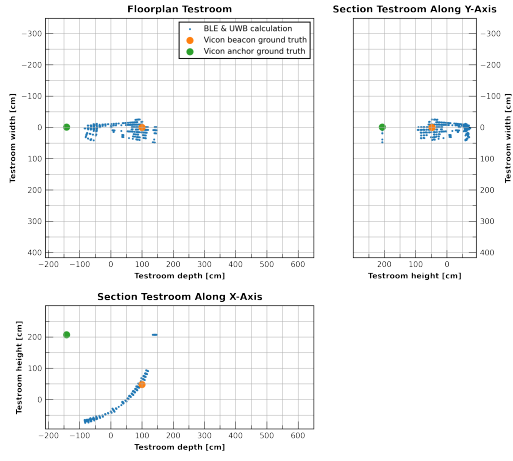


Figure F.11.: 08 Mai Experiment  
Position 2 Position Plot

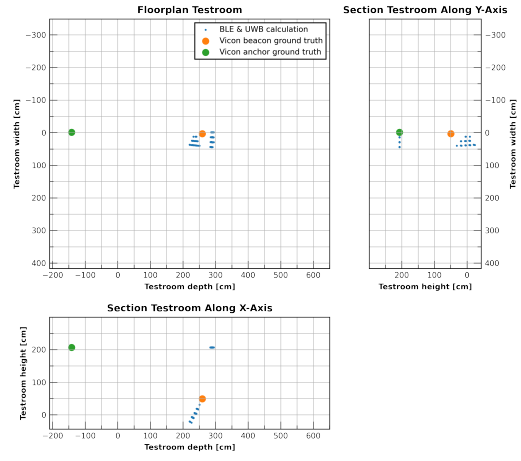


Figure F.12.: 08 Mai Experiment  
Position 3 Position Plot

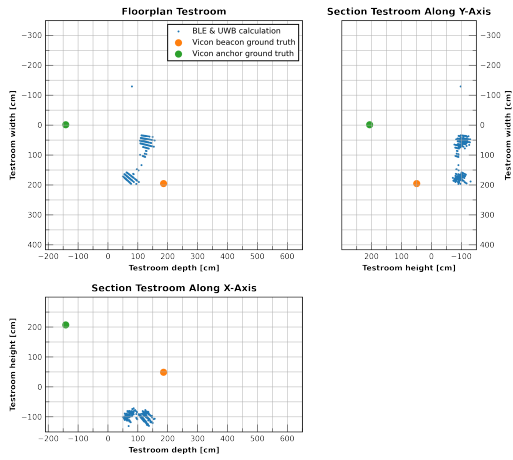


Figure F.13.: 08 Mai Experiment  
Position 4 Position Plot

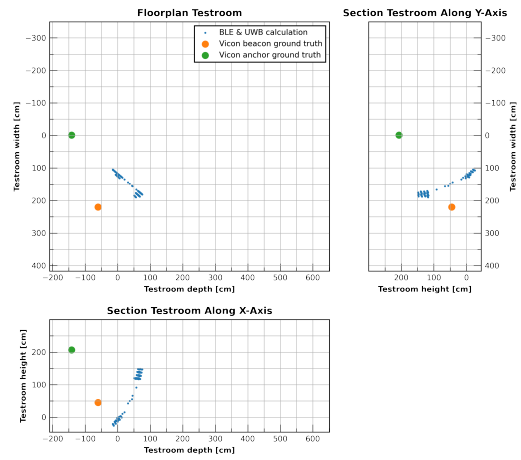


Figure F.14.: 08 Mai Experiment  
Position 5 Position Plot

F. Remaining Plots

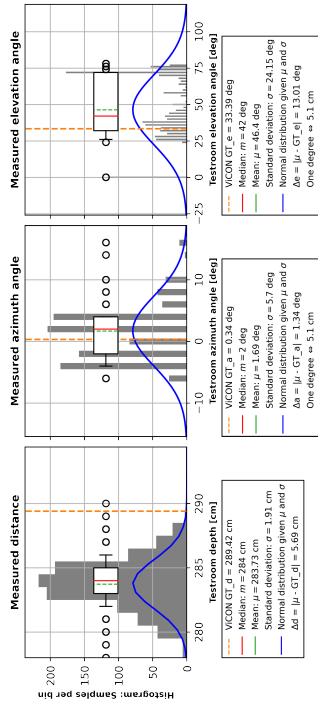


Figure F.15.: 08 Mai Experiment Position 2 Histogram Plot

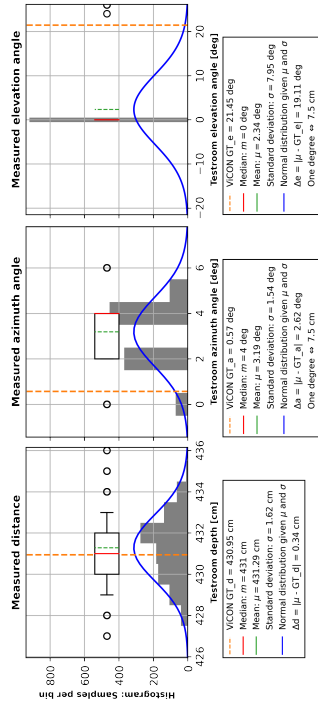


Figure F.16.: 08 Mai Experiment Position 3 Histogram Plot

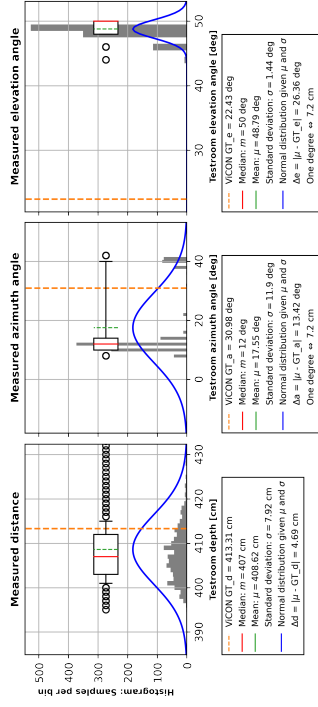


Figure F.17.: 08 Mai Experiment Position 4 Histogram Plot

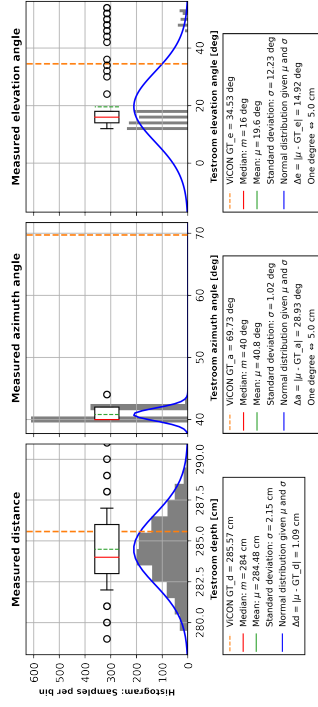


Figure F.18.: 08 Mai Experiment Position 5 Histogram Plot

## F. Remaining Plots

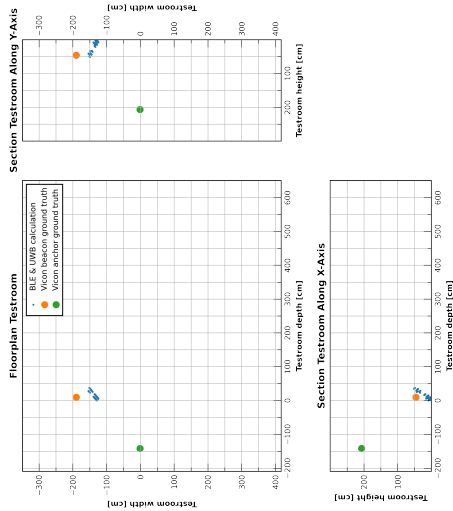


Figure F.19.: 08 Mai Experiment  
Position 8 Position Plot

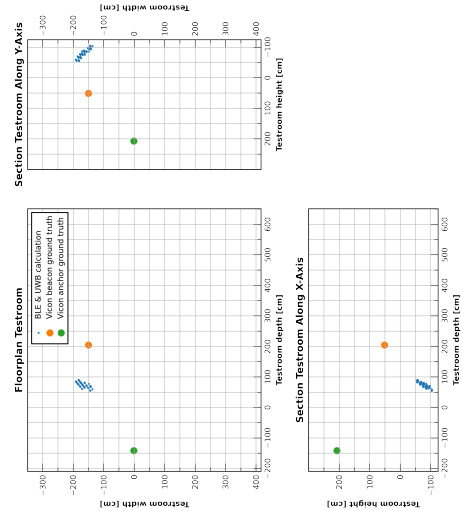


Figure F.20.: 08 Mai Experiment  
Position 9 Position Plot

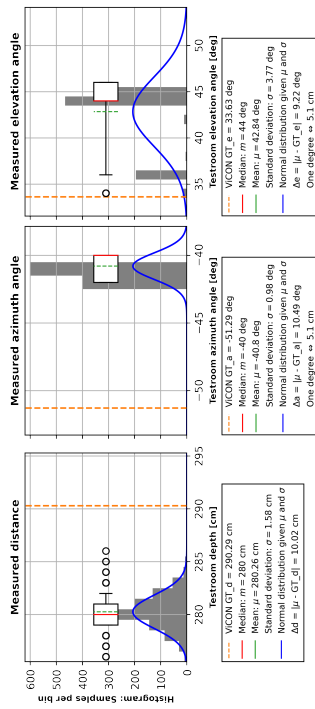


Figure F.21.: 08 Mai Experiment  
Position 8 Histogram Plot

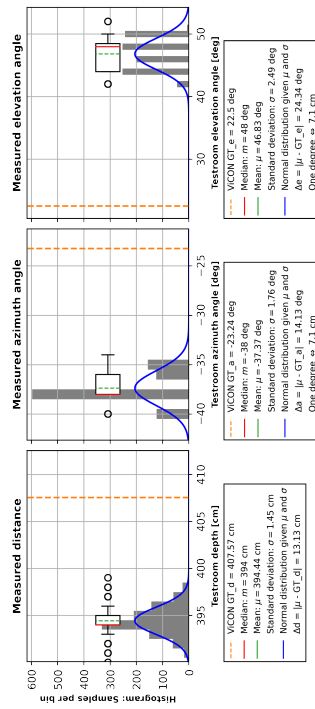


Figure F.22.: 08 Mai Experiment  
Position 9 Histogram Plot

## F. Remaining Plots

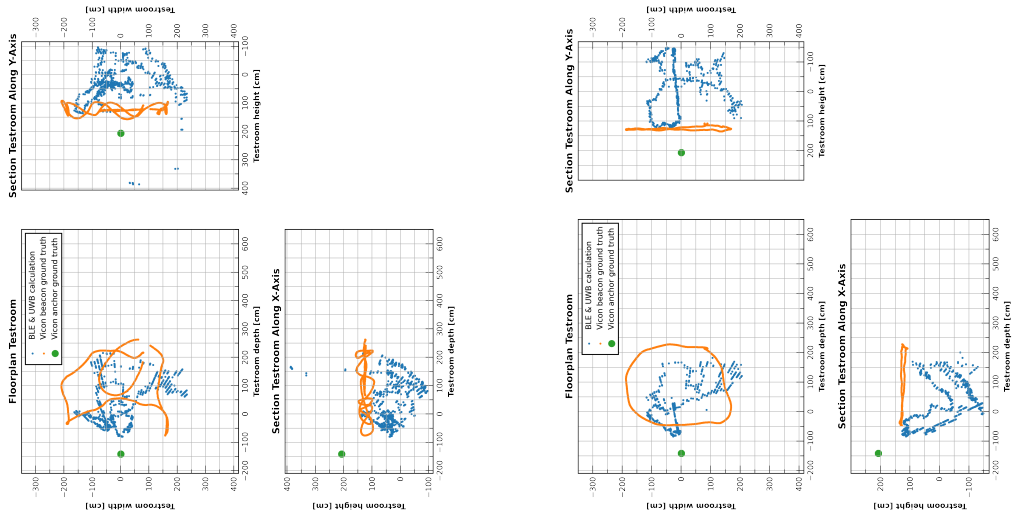


Figure F.23.: 08 Mai Dynamic Experiment 1 Plot

Figure F.24.: 08 Mai Dynamic Experiment 2 Plot

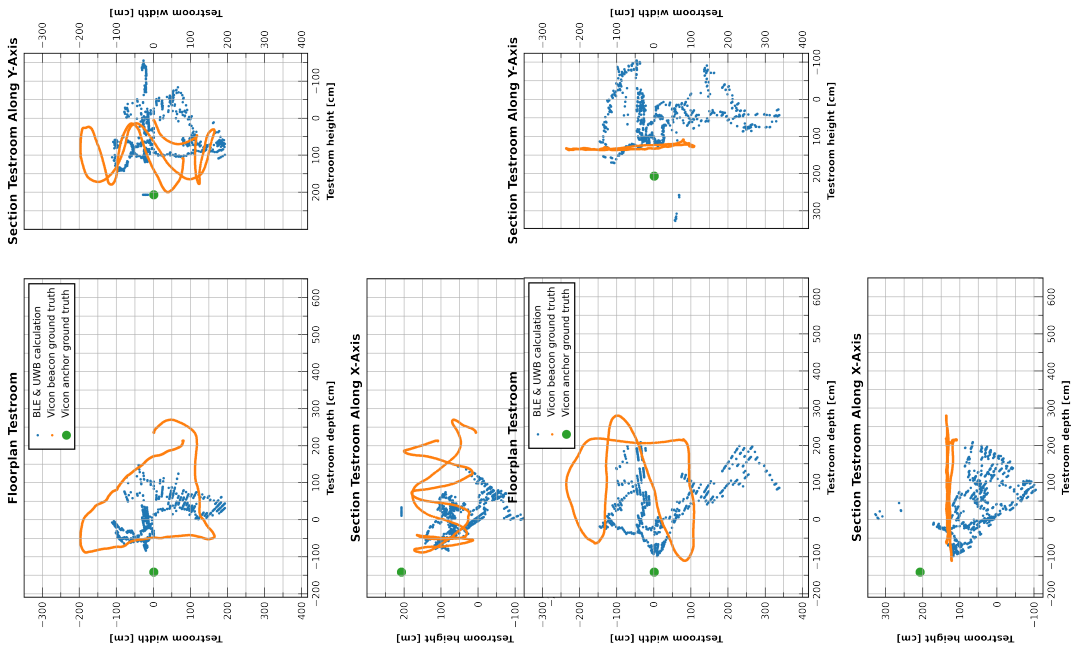


Figure F.25.: 08 Mai Dynamic Experiment 3 Plot

Figure F.26.: 08 Mai Dynamic Experiment 4 Plot



# Glossary

**Octet** Unit of digital information in the fields of computing and telecommunications. An octet of bits is **eight** bits. Although today a byte and an octet can be used interchangeably in most fields there still is some ambiguity to the term byte since it has historically been used for storage units of varying size. Thus the term octet stuck for transmissions to clearly define the amount sent..

# Bibliography

- [1] U-Blox. (2021) Xplr-aoa explorer kits - bluetooth indoor direction finding. [Accessed 20-April-2022]. [Online]. Available: [https://www.u-blox.com/en/ubx-viewer/view/XPLR-AOA-Explorer-kits\\_UserGuide\\_UBX-21004616?url=https%3A%2F%2Fwww.u-blox.com%2Fsites%2Fdefault%2Ffiles%2FXPLR-AOA-Explorer-kits\\_UserGuide\\_UBX-21004616.pdf](https://www.u-blox.com/en/ubx-viewer/view/XPLR-AOA-Explorer-kits_UserGuide_UBX-21004616?url=https%3A%2F%2Fwww.u-blox.com%2Fsites%2Fdefault%2Ffiles%2FXPLR-AOA-Explorer-kits_UserGuide_UBX-21004616.pdf)
- [2] O. T. Renato Cicchetti, Emanuela Miozzi, “Wideband and uwb antennas for wireless applications: A comprehensive review,” in *International Journal of Antennas and Propagation*, vol. 2017, 2017.
- [3] S. Gansemer, U. Großmann, and S. Hakobyan, “Rssi-based euclidean distance algorithm for indoor positioning adapted for the use in dynamically changing wlan environments and multi-level buildings,” in *2010 International Conference on Indoor Positioning and Indoor Navigation*, 2010, pp. 1–6.
- [4] J. Larranaga, L. Muguira, J.-M. Lopez-Garde, and J.-I. Vazquez, “An environment adaptive zigbee-based indoor positioning algorithm,” in *2010 International Conference on Indoor Positioning and Indoor Navigation*, 2010, pp. 1–8.
- [5] V. Namboodiri, M. DeSilva, K. Deegala, and S. Ramamoorthy, “An extensive study of slotted aloha-based rfid anti-collision protocols,” *Computer Communications*, vol. 35, no. 16, pp. 1955–1966, 2012. [Online]. Available: <https://www.sciencedirect.com/science/article/pii/S0140366412001776>
- [6] M. S. Bargh and R. de Groote, “Indoor localization based on response rate of bluetooth inquiries.” New York, NY, USA: Association for Computing Machinery, 2008, p. 49–54. [Online]. Available: <https://doi.org/10.1145/1410012.1410024>
- [7] G. Conte, M. De Marchi, A. Nacci, V. Rana, and D. Sciuto, “Bluesentinel: A first approach using ibeacon for an energy efficient occupancy detection system,” 11 2015.

## Bibliography

- [8] Y. Shen and M. Z. Win, “Fundamental limits of wideband localization— part i: A general framework,” *IEEE Transactions on Information Theory*, vol. 56, no. 10, pp. 4956–4980, 2010.
- [9] S. He, H. Long, and W. Zhang, “Multi-antenna array-based aoa estimation using bluetooth low energy for indoor positioning,” in *2021 7th International Conference on Computer and Communications (ICCC)*, 2021, pp. 2160–2164.
- [10] Z. Hajiakhondi-Meybodi, M. Salimibeni, K. N. Plataniotis, and A. Mohammadi, “Bluetooth low energy-based angle of arrival estimation via switch antenna array for indoor localization,” in *2020 IEEE 23rd International Conference on Information Fusion (FUSION)*, 2020, pp. 1–6.
- [11] S. Monfared, A. Delepaut, M. Van Eeckhaute, P. De Doncker, and F. Horlin, “Iterative localization method using aoa for iot sensor networks,” in *2019 IEEE 89th Vehicular Technology Conference (VTC2019-Spring)*, 2019, pp. 1–6.
- [12] G. Wang, Y. Xu, F. Tong, J. Pan, and S. Shen, “Modeling and analyzing single anchor localization for internet of things,” in *ICC 2019 - 2019 IEEE International Conference on Communications (ICC)*, 2019, pp. 1–6.
- [13] B. Großwindhager, M. Rath, J. Kulmer, M. S. Bakr, C. A. Boano, K. Witrissal, and K. Römer, “Salma: Uwb-based single-anchor localization system using multipath assistance,” ser. SenSys '18, New York, NY, USA, 2018, p. 132–144. [Online]. Available: <https://doi.org/10.1145/3274783.3274844>
- [14] T. Wang, H. Zhao, and Y. Shen, “An efficient single-anchor localization method using ultra-wide bandwidth systems,” *Applied Sciences*, vol. 10, no. 1, p. 57, 2019.
- [15] T. Instruments. (2021) Bluetooth low energy scanning and advertising. [Accessed 20-April-2022]. [Online]. Available: [https://dev.ti.com/tirex/explore/content/simplelink\\_academy\\_cc13x2\\_26x2sdk\\_5\\_20\\_02\\_00/modules/ble5stack/ble\\_scan\\_adv\\_basic/ble\\_scan\\_adv\\_basic.html#advertising](https://dev.ti.com/tirex/explore/content/simplelink_academy_cc13x2_26x2sdk_5_20_02_00/modules/ble5stack/ble_scan_adv_basic/ble_scan_adv_basic.html#advertising)
- [16] M. Woolley, *Bluetooth Direction Finding - A Technical Overview*, Bluetooth SIG, Oct. 2021.
- [17] Y. Wang, Q. Ye, J. Cheng, and L. Wang, “Rssi-based bluetooth indoor localization,” in *2015 11th International Conference on Mobile Ad-hoc and Sensor Networks (MSN)*, 2015, pp. 165–171.
- [18] MathWorks. (2021) Bluetooth location and direction finding - angle of arrival / departure. [Accessed 20-April-2022]. [Online]. Available: [https://ch.mathworks.com/help/bluetooth/ug/bluetooth-direction-finding.html;jsessionid=771f33ada5b67dd85931f5d23ecf#mw\\_82903b60-b773-45c2-a537-31bb3d6d8864](https://ch.mathworks.com/help/bluetooth/ug/bluetooth-direction-finding.html;jsessionid=771f33ada5b67dd85931f5d23ecf#mw_82903b60-b773-45c2-a537-31bb3d6d8864)
- [19] ——. (2021) Bluetooth le packet structure. [Accessed 20-April-2022]. [Online]. Available: [https://ch.mathworks.com/help/bluetooth/ug/bluetooth-packet-structure.html#mw\\_d580926e-5e4b-4e45-9884-e5e7476e4948](https://ch.mathworks.com/help/bluetooth/ug/bluetooth-packet-structure.html#mw_d580926e-5e4b-4e45-9884-e5e7476e4948)

## Bibliography

- [20] Google. (2021) Git repository - google eddystone. [Accessed 20-April-2022]. [Online]. Available: <https://github.com/google/eddystone>
- [21] U-Blox. (2021) Git repository - c209 tags. [Accessed 20-April-2022]. [Online]. Available: <https://github.com/u-blox/c209-aoa-tag>
- [22] Y. Rahayu, T. A. Rahman, R. Ngah, and P. Hall, "Ultra wideband technology and its applications," in *2008 5th IFIP International Conference on Wireless and Optical Communications Networks (WOCN '08)*, 2008.
- [23] Quorvo. (2021) DWM3000 - User Manual. [Accessed 20-April-2022]. [Online]. Available: <https://www.decawave.com/wp-content/uploads/2021/05/DW3000-User-Manual-1.pdf>
- [24] Zephyr. (2021) Zephyr project documentation. [Accessed 20-April-2022]. [Online]. Available: <https://docs.zephyrproject.org/latest/index.html>
- [25] Apache. (2004) Apache license. [Accessed 20-April-2022]. [Online]. Available: <https://www.apache.org/licenses/LICENSE-2.0>
- [26] UBlox. (2022) u-blox NORA-B1 Bluetooth® 5.2 Modules. [Accessed 20-April-2022]. [Online]. Available: <https://www.mouser.ch/new/u-blox/ublox-nora-b1-modules/>
- [27] Quorvo. (2021) DWM3000 - 6.5 8.0 GHz Ultra-Wideband (UWB) Module. [Accessed 20-April-2022]. [Online]. Available: <https://www.qorvo.com/products/p/DWM3000>
- [28] STM. (2022) iNEMO 3D accelerometer and 3D gyroscope. [Accessed 20-April-2022]. [Online]. Available: <https://www.st.com/en/mems-and-sensors/lsm6dsv16x.html>
- [29] V. Niculescu. How to
- [30] C. V. M. M. S. K. Robin Hunziker, Silvano Cortesi, "SmartPatch - Indoor Localization and Audio Acquisition," 2022.
- [31] D. E. Knuth, *The TeXbook*. Addison-Wesley, 1984.
- [32] H. Kaeslin, *Digital Integrated Circuit Design: From VLSI Architectures to CMOS Fabrication*. Cambridge University Press, Apr. 2008.
- [33] D. Hankerson, S. Vanstone, and A. Menezes, *Guide to Elliptic Curve Cryptography*, ser. Springer Professional Computing. Springer, 2004.
- [34] NIST, *Advanced Encryption Standard (AES) (FIPS PUB 197)*, National Institute of Standards and Technology, Nov. 2001.
- [35] P. Rogaway, M. Bellare, J. Black, and T. Krovetz, "OCB: A Block-Cipher Mode of Operation for Efficient Authenticated Encryption," in *ACM Conference on Computer and Communications Security*, 2001, pp. 196–205.

## Bibliography

- [36] Xilinx. (2011, Oct.) 7 Series FPGAs Configuration - User Guide. UG470 (v1.2) October 26, 2011. [Online]. Available: [http://www.xilinx.com/support/documentation/user\\_guides/ug470\\_7Series\\_Config.pdf](http://www.xilinx.com/support/documentation/user_guides/ug470_7Series_Config.pdf)
- [37] Wikipedia, "Isaac newton — wikipedia, the free encyclopedia," 2012, [Online; accessed 1-October-2012]. [Online]. Available: [http://en.wikipedia.org/w/index.php?title=Isaac\\_Newton&oldid=514997436](http://en.wikipedia.org/w/index.php?title=Isaac_Newton&oldid=514997436)
- [38] J. K. B. SIG. (2017) Bluetooth low energy – it starts with advertising. [Accessed 20-April-2022]. [Online]. Available: <https://www.bluetooth.com/blog/bluetooth-low-energy-it-starts-with-advertising>
- [39] I. . T. G. . (TG4). (2011) Ieee standard for local and metropolitan area networks. [Accessed 20-April-2022]. [Online]. Available: <https://www.ieee802.org/15/pub/TG4.html>
- [40] AUTOHOR. (2021) Title. [Accessed 20-April-2022]. [Online]. Available: WEBPAGE
- [41] "Ieee draft standard for low-rate wireless networks," *IEEE P802.15.4-REVd/D06*, March 2020, pp. 1–945, 2020.